



1-1-2013

Mechanical Characterization Of Composite Repairs For Fiber-Glass Wind Turbine Blades

Tanveer Singh Chawla

Follow this and additional works at: <https://commons.und.edu/theses>

 Part of the [Mechanical Engineering Commons](#)

Recommended Citation

Chawla, Tanveer Singh, "Mechanical Characterization Of Composite Repairs For Fiber-Glass Wind Turbine Blades" (2013). *Theses and Dissertations*. 1517.

<https://commons.und.edu/theses/1517>

This Dissertation is brought to you for free and open access by the Theses, Dissertations, and Senior Projects at UND Scholarly Commons. It has been accepted for inclusion in Theses and Dissertations by an authorized administrator of UND Scholarly Commons. For more information, please contact zeinebyousif@library.und.edu.

MECHANICAL CHARACTERIZATION OF COMPOSITE REPAIRS FOR FIBER-
GLASS WIND TURBINE BLADES

by

Tanveer Singh Chawla
Bachelor of Engineering, Guru Nanak Dev Engineering College, 1996
Master of Science, Wayne State University, 2008

A Dissertation

Submitted to the Graduate Faculty
of the
University of North Dakota
in partial fulfillment of the requirements

for the degree of
Doctor of Philosophy

Grand Forks, North Dakota

December

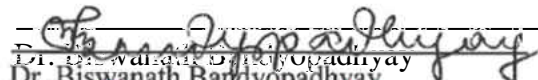
2013

Copyright 2013 Tanveer Singh Chawla


This dissertation, submitted by Tanveer Singh Chawla in partial fulfillment of the requirements for the Degree of Doctor of Philosophy from the University of North Dakota, has been read by the Faculty Advisory Committee, after whom the work has been done, and is hereby approved.



Dr. Matthew N Cavalli




Dr. Biswanath Bandyopadhyay



Dr. George Bibel



Dr. Brian Tande



Dr. Edward Kolodka

This dissertation is being submitted by the appointed advisory committee as having met all of the requirements of the School of Graduate Studies at the University of North Dakota and is hereby approved.



Dr. Wayne Swisher

Dean of the School of Graduate Studies

December 10, 2013

Date

Date

PERMISSION

Title	Mechanical Characterization of Composite Repairs for Fiber-Glass Wind Turbine Blades
Department	Mechanical Engineering
Degree	Doctor of Philosophy

In presenting this dissertation in partial fulfillment of the requirements for a graduate degree from the University of North Dakota, I agree that the library of this University shall make it freely available for inspection. I further agree that permission for extensive copying for scholarly purposes may be granted by the professor who supervised my dissertation work or, in his absence, by the Chairperson of the department or the dean of the School of Graduate Studies. It is understood that any copying or publication or other use of this dissertation or part thereof for financial gain shall not be allowed without my written permission. It is also understood that due recognition shall be given to me and to the University of North Dakota in any scholarly use which may be made of any material in my dissertation.

Tanveer Singh Chawla
08/15/2013

TABLE OF CONTENTS

LIST OF FIGURES	vii
LIST OF TABLES	x
ACKNOWLEDGEMENTS	xi
ABSTRACT	xii
CHAPTER	
I. INTRODUCTION	
Repair Methods for FRP Composites	1
Patch Repairs	2
Scarf Repairs	2
Step Repairs	3
Testing of FRP Composite Repairs	4
Mode I Testing	5
Fatigue Testing	7
Mixed-Mode (Mode I & Mode II) Testing	10
II. EVALUATION OF GFRP REPAIRS BY MODE I TESTING	
Introduction	13
Resin Selection	14
Specimen Fabrication	14
Testing	19

Calculations	20
Results and Discussion	22
Grinding Variation Study	30
Conclusions	36
III. EVALUATION OF GFRP REPAIRS BY FATIGUE TESTING	
Introduction	37
Specimen Fabrication	37
Fatigue Calculations and Testing	39
Results and Discussion	41
IV. STUDY OF REPAIR PARAMETERS BY MIXED MODE I – MODE II TESTING	
Specimen Manufacturing and Preparation	45
Initial Testing Specimens	45
Subsequent Testing Specimens.....	46
Testing and Calculations	50
Results and Discussion	54
Initial Testing	54
Subsequent Testing	58
Conclusions	66
CONCLUSIONS	68
REFERENCES	74

LIST OF FIGURES

Figure	Page
1.1. Patch Repair [4]	2
1.2. Scarf Repair [4]	3
1.3. Step Repair [4]	4
2.1. DCB Specimen	15
2.2. VARTM set-up before infusion	16
2.3. VARTM infusion package	16
2.4. Straight rule along Combi plies' 0° direction (1-direction)	17
2.5. Straight rule along Combi plies' 90° direction	17
2.6. Experimental set-up for DCB testing	20
2.7. G_{Ic}'/G_{Ic0}' vs crack length for main blade resin, MB-A	23
2.8. G_{Ic}'/G_{Ic0}' vs crack length for current repair resin, MB-B	23
2.9. Surface morphologies after crack propagation	24
2.10. Fiber bridging in case of MB-A (main blade resin)	25
2.11. Grinding difference in case of NRR1, NRR4 and NRR5 resins (a) Complete top ply ground off (b) Partial top ply ground off	25
2.12. G_{Ic}'/G_{Ic0}' vs crack length for candidate resin, NRR1	26
2.13. G_{Ic}'/G_{Ic0}' vs crack length for candidate resin, NRR2	27
2.14. G_{Ic}'/G_{Ic0}' vs crack length for candidate resin, NRR3	27
2.15. G_{Ic}'/G_{Ic0}' vs crack length for candidate resin, NRR4	28
2.16. G_{Ic}'/G_{Ic0}' vs crack length for candidate resin, NRR5	28
2.17. G_{Ic}'/G_{Ic0}' vs crack length for candidate resin, NRR6	29

2.18. Fractured surfaces of NRR3 specimens with dry patches in CSM	29
2.19. G_{Ic}'/G_{Ic0}' vs crack length for resin NRR1 with partial ply ground off	31
2.20. G_{Ic}'/G_{Ic0}' vs crack length for resin NRR4 with partial top ply ground off	31
2.21. G_{Ic}'/G_{Ic0}' vs crack length for resin NRR5 with partial top ply ground off	32
2.22. Comparison of fracture toughness values of NRR1 specimens with (i) whole top ply ground off (NRR1-#) (ii) partial top ply ground off (NRR1-#*)	33
2.23. Comparison of fracture toughness values of NRR4 specimens with (i) whole top ply ground off (NRR4-#) (ii) partial top ply ground off (NRR4-#*)	34
2.24. Comparison of fracture toughness values of NRR5 specimens with (i) whole top ply ground off (NRR5-#) (ii) partial top ply ground off (NRR5-#*)	34
2.25. Normalized fracture toughness values from crack initiation at $a = 30$ mm for (i) complete top ply ground off case, NRR# (ii) partial top ply ground off case, NRR#*	35
3.1. Fatigue tensile test specimen configuration (side view, not to scale)	38
3.2. Actual fatigue test specimen	39
3.3. Experimental set-up of tension-tension fatigue testing (dimensions in mm)	40
3.4. Strain-Life plot for ground (MB-B ground) and unground (MB-B) specimens	41
3.5. Stress-Life plot for ground (MB-B ground) and unground (MB-B) specimens	42
3.6. Strain –Life plot for unground specimens repaired with MB-B, NRR1, NRR4 and NRR6 repair resins	43
3.7. Stress –Life plot for unground specimens repaired with MB-B, NRR1, NRR4 and NRR6 repair resins	44
4.1. Specimen details for mixed mode I – mode II test [61]	46
4.2. Mixed-mode specimen manufacturing (a) VARTM (b) Grinding (c) repair surface preparation (d) resin application (e) removal of voids	50
4.3. Test fixture and parameters of mixed-mode test [61]	51
4.4. Mixed mode I – mode II test snapshot	52
4.5. (a) Preliminary mixed mode I – mode II testing results for current blade repair resin MB-B	54

4.5. (b) Preliminary mixed mode I – mode II testing results for new repair resin candidate NRR4	55
4.6. Fiber bridging in NRR6 (specimen A), NRR4 (specimen B) and MB-B (specimen C) in mixed mode I – mode II ($G_{II}/G_c = 0.2$) test	57
4.7. Fracture toughness values at crack initiation for MB-B, NRR4 and NRR6	57
4.8. Parent plate with (a) complete top ply ground off (b) partial top ply ground off	58
4.9. Delamination fracture toughness values for MB-B with whole top ply of parent plate ground off	59
4.10. Delamination fracture toughness values for MB-B with partial top ply of the parent plate ground off	60
4.11. Delamination fracture toughness values for NRR4' with whole top ply of parent plate ground off	60
4.12. Delamination fracture toughness values for NRR4' with partial top ply of the parent plate ground off	61
4.13. Fracture toughness values for MB-B and NRR4' at different grinding levels under mode II 20% loads (1 Ply ~ Complete top ply ground off, 0.5 Ply ~ Partial top ply ground off)	63
4.14. Fracture toughness values for MB-B and NRR4' at different grinding levels under mode II 50% loads (1 Ply ~ Complete top ply ground off, 0.5 Ply ~ Partial top ply ground off)	63
4.15. Images of surfaces fractured under different mixed mode I – mode II loads	64

LIST OF TABLES

Table	Page
2.1. Compositions of repair resins	14
2.2. Mode I test specimen lay-up, materials used and curing details	15
2.3. Recorded values for new repair resins	18
2.4. Consolidated mode I fracture testing results (top ply ground off completely)	30
2.5. Consolidated mode I fracture testing results (top ply ground off partially)	33
3.1. Fatigue specimen lay-up, curing and post curing details	38
4.1. Initial mixed mode I – mode II specimen lay-up, materials used and curing details	45
4.2. Subsequent mixed mode I – mode II specimen lay-up, materials used and curing details	48
4.3. Fracture toughness ($G_{II}/G = 0.2$) values for MB-B	56
4.4. Fracture toughness ($G_{II}/G = 0.2$) values for NRR4	56
4.5. Estimated load values calculated using Equation 4.11 for different values of h	62

ACKNOWLEDGEMENTS

I would like to thank my advisor, Dr. Matthew Cavalli, for his patience, guidance and support during the research and writing of this dissertation. Besides my advisor, I wish to express my sincere gratitude to the rest of the dissertation committee: Dr. Brian Tande, Dr. Biswanath Bandyopadhyay, Dr. George Bibel and Dr. Edward Kolodka, for their assistance and supervision.

I would also like to thank the Department of Mechanical Engineering at University of North Dakota and LM Windpower who made this research possible. I am grateful to Mr. John Jenó (Senior Manager, Engineering & CI, LM Windpower) for sharing his invaluable expertise and experience with composite materials.

Finally, I would like to thank my friends and family who have stood steadfast by me and provided inspiration throughout this work.

ABSTRACT

While in service, wind turbine blades experience various modes of loading. An example is impact loading in the form of hail or bird strikes, which might lead to localized damage or formation of cracks a few plies deep on the blade surface. One of the methods to conduct repairs on wind turbine blades that are damaged while in service is hand lay-up of the repair part after grinding out the damaged portion and some of its surrounding area. The resin used for such repairs usually differs from the parent plate resin in composition and properties such as gel time, viscosity, etc. As a result the properties of the repaired parts are not the same as that of the undamaged blades. Subsequent repetitive loading can be detrimental to weak repairs to such an extent so as to cause delamination at the parent-repair bondline causing the repairs to eventually fall off the blade. Thus the strength and toughness of the repair are of critical importance.

Initial part of this work consists of an effort to increase repair strength by identifying an optimum hand layup repair resin for fiberglass wind turbine blades currently being manufactured by a global company. As delamination of the repair from the parent blade is a major concern and unidirectional glass fibers along with a polymer resin are used to manufacture blades under consideration, testing method detailed in ASTM D 5528 (Test Method for Mode I Interlaminar Fracture Toughness of Unidirectional Fiber-Reinforced Polymer Matrix Composites) was followed to determine propagation fracture toughness values of the prospective vinyl ester repair resin candidates. These values were compared to those for a base polyester repair resin used by the company. Experimental procedure

and results obtained from the above mentioned testing using double cantilever beam (DCB) specimens are detailed. Three new repair resins were shortlisted through mode I testing. It was also found that variation in the depth of the ground top ply of the parent part affects the propagation fracture toughness values of the repair. Repairs conducted on surfaces with partially ground top plies possess higher fracture toughness values than those conducted on surfaces with complete top plies ground off.

The three top repair resin candidates were then evaluated against the base repair resin under fatigue loading. The specimen configuration and testing method were chosen so as to be able to test hand layup repairs under tension – tension cyclic loading. It was observed that all three new repair resins perform better than the base repair resin. The selection of the optimum repair resin was based on results from mode I and fatigue testing. Global manufacturing regulations and standards were also of prime concern. The final new repair resin is being used by the company in all of its plants over the globe.

The balance of this work involves study of the effect of mixed mode I – mode II loading on the strength of repairs conducted on fiber reinforced composite parts using hand layup technique. The specimens for this part were similar to those manufactured for mode I testing but with different dimensions and layup. They were made and tested in accordance with ASTM D 6671 (Standard Test Method for Mixed Mode I – Mode II Interlaminar Fracture Toughness of Unidirectional Fiber Reinforced Polymer Matrix Composites). Comparison was made between the fracture toughness of the above chosen optimum repair resin and the base repair resin. At least two levels of mode mixture G_{II}/G (Mode II fracture toughness / Mode I and II fracture toughness) were examined. Also, two levels of grinding were considered (complete ply vs. partial ply ground off) in order

to establish the influence of varying top-ply grinding depths on the strength of hand layup repairs conducted on fiberglass composite structures.

The results of this work have the potential to improve the repair process for current fiberglass wind turbine blades.

To Aarav, Korvin and Hazel.

CHAPTER I

INTRODUCTION

Repair Methods for FRP Composites

Fiber reinforced polymer (FRP) composites are not only lightweight, but also possess good mechanical and thermal properties [1]. Their resistance to corrosion and fatigue has made them suitable materials for aeronautical applications and also for alternate energy production such as in manufacturing of wind turbine blades. Despite their high level of performance, they are susceptible to impact damage during the time of their service. The damage may also be due to moisture or hydraulic fluids absorption [2]. Military aerospace vehicles made of composites may suffer damage in war whereas blades of wind turbines might show presence of cracks due to severe fatigue loads in extreme weather conditions. Whatever the case may be, it has become necessary for manufacturers to develop techniques for low cost and rapid repair of components made of composite materials. The repair method used depends not only on the extent of damage but also on the required properties such as thickness, strength and aerodynamic profile of the final repaired product [3]. To be effective, the structural repair should be capable of supporting the applied loads and transmitting the resultant stresses across the repaired area. The prevalent methods of repair of composites are patch repair, taper sanded (scarf) repair and step sanded repair [4].

Patch Repairs

Patch repairs involve the use of filler plies (Figure 1) to make up for the thickness of the original laminate and repair patches are either bonded adhesively or mechanically fastened to the laminate surface externally.

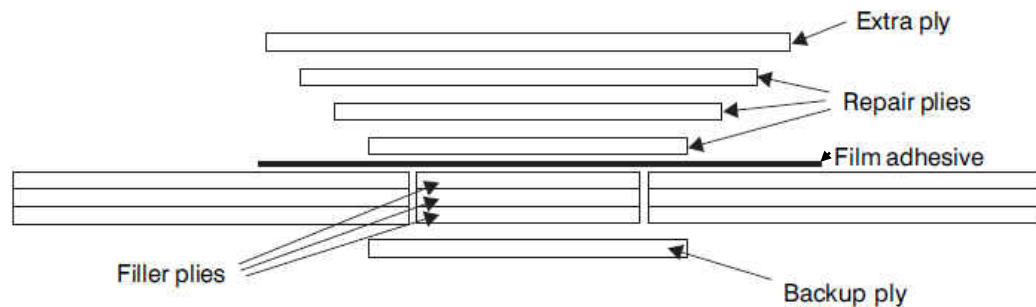


Figure 1.1. Patch repair [4]

Different types of lay-ups may be used for repairs in this case. Pre-preg plies may be used and cured simultaneously with the adhesive. Application of pre-cured plies alternating with epoxy based paste adhesive layers is another alternative. Parts may also be manufactured by preforming and later bonded to the repair area to fit the repair contour [5]. Repair contours possessing double curvatures may be repaired by wet lay-ups consisting of plies similar to parent laminate with two-part (resin and initiator) systems. Though patch repairs are practically very easy and require minimum preparation, the disadvantages are that the repaired laminate is heavier and thicker than the original and the surface has to be very carefully prepared for proper adhesion [5].

Scarf Repairs

Scarf repairs are time-consuming and more difficult than patch repairs due to high skill and precision needed for accurate machining of the damaged structure. In this type of repair, the area of the damaged portion and that around it is sanded to expose each layer

of the laminate (Figure 2). Sometimes a filler ply may be added in addition to the repair plies to have a flatter surface. A wet lay-up is preferred as there might be fitting problems with the pre-cured ones. As in the case of patch repairs, the stacking sequence of the repair plies is the same as that of the parent laminate and an extra ply is added at the top of the repair plies to increase the overall strength and reduce creep as much as possible [3].

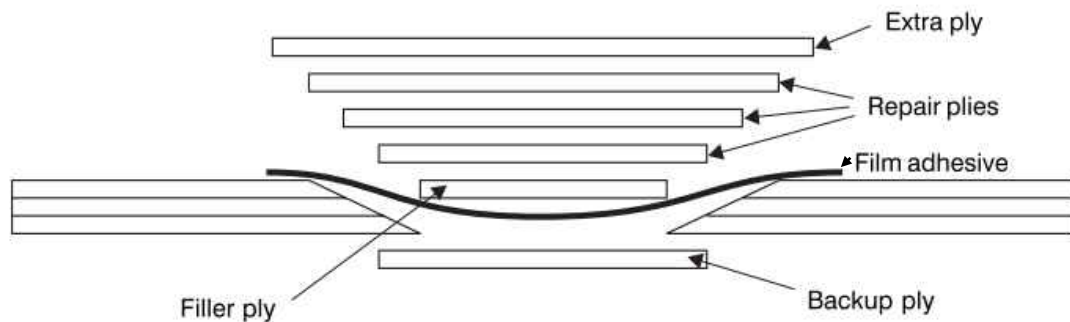


Figure 1.2. Scarf repair [4]

Curing of the lay-up is carried out by keeping the repair portion at room temperature under atmospheric pressure or by vacuum bagging in an autoclave or simply vacuum bagging in the open [3]. The advantage over patch repair is that the laminate repaired by this technique is only a little thicker than the original and a straighter load path is produced as each ply overlaps the corresponding ply being repaired resulting in a uniform shear stress distribution. The amount of strength restored to the original part varies with changes in parameters such as scarf angles, material used and depth of repair, etc.

Step Repairs

In step repair, as the name suggests, the damaged plies are sanded such that a flat face of the ply is exposed giving the laminate a 'stair-like' appearance (Figure 3). The steps are

typically 25-50 mm per layer and the sanding increases the roughness of surface to be bonded thus increasing adhesion with the repair resin.

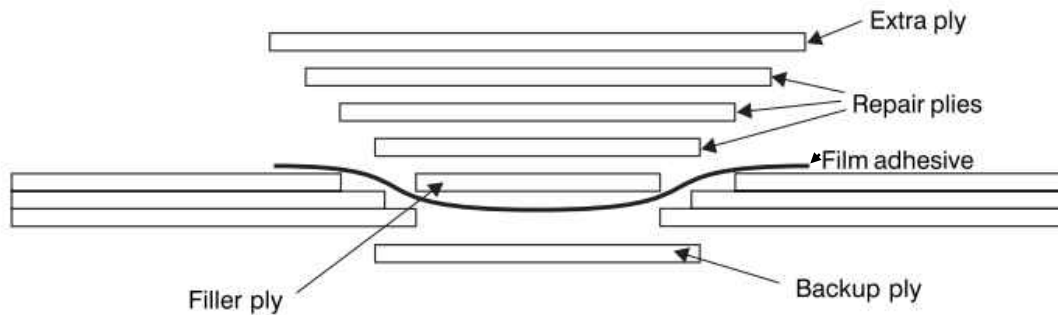


Figure 1.3. Step repair [4]

The resultant laminate is almost the same as that produced in scarf repairs as good bonds are achieved due to exposure of fibers to the resin but this method requires considerable skill.

Testing of FRP Composite Repairs

Testing of repaired composites is very necessary not only for evaluating the quality of the repair but also for quantitatively analyzing the differences introduced such as reduction in values of mechanical properties that reflect on the overall strength of the parent laminate. Thus, performing tests on repairs carried out on composites has become an integral part of analyzing repairs. The choice of the type of test to be conducted depends upon the property of the repair being tested. Repairs conducted on wind turbine blades are tested at many levels in order to be certified. These levels and testing modes are in accordance with certain standards [6 – 12] developed mainly in Europe [13] in the early 21st century. To test the fracture toughness of materials many mechanical test methods have been developed. Double cantilever beam (DCB) specimens are used for testing materials under pure mode I (opening mode) and mixed mode I – mode II loading. The end notched

flexure (ENF) test is currently under ASTM review [14] and is used for testing specimens under pure mode II (shearing mode) loading. Tests developed to test composite coupons under cyclic loading include the in-plane tension/tension fatigue test [15] for gathering stress-cycles (S-N) data and the fatigue crack growth/toughness test method [16] for obtaining delamination initiation toughness-cycles (G-N) data. Some common test methods used for evaluation of fracture toughness of FRP composites and composite repairs are discussed in the next few sections.

Mode I Testing

Damage in continuous fiber reinforced composites may occur as delamination, fiber failure, matrix failure or fiber matrix debonding [3]. Delamination or separation of different plies in a laminate is a common type of damage due to low velocity impacts and cyclic loading [17]. The strain energy release rate accompanied by delamination due to mode I loading is usually measured by conducting tests using a Double Cantilever Beam (DCB) specimen [18-21]. The testing method [18] that has been used to conduct work for this report will be described in detail in a subsequent chapter. Mode I testing has been in more focus as the energy required to initiate a crack under mode I loading is less than that under mode II loading [22]. Perrin *et al* [23] used DCB specimens to evaluate and compare mode I interlaminar fracture toughness values of unidirectional glass fiber polypropylene composites manufactured with varying molding temperatures and cooling rates. In a second part of the same study the test temperatures were also varied in order to study the effect of change in environmental temperature on crack propagation. Their results indicated a strong influence of molding conditions on the fracture toughness of composite laminates. Various studies involving mode I testing have been carried out to

improve interlaminar fracture toughness. Tzetzis & Hogg [24] studied the bondline fracture characteristics of composite repairs with mode I testing and proved that the introduction of carbon and polyester veils at the bondline improved the quality of the repairs significantly. Fracture toughness values of the repairs with and without the multidirectional fibers at the repair – parent plate bondline were measured and compared through R-curves. An R-curve is obtained by plotting the total energy dissipation rate against the crack size. Introduction of the veils consisting of multidirectional fibers leads to the phenomena of crack arrest and bridging that increase the strain energy release rate. Bader *et al* [25] used mode I testing to compare the fracture toughness of repairs conducted with one part adhesive, ethylcyanoacrylate (ECA), to the fracture toughness of repairs conducted with two part epoxy based system, diglycidyl ether of bisphenol A (DGEBA) cured with 4,4'-methylene-bis(aminocyclohexane) (PACM). In both cases, the repairs possessed higher fracture toughness values as compared to the original carbon fiber epoxy composite parts. As stated earlier, fracture toughness values of composites are governed by various factors such as ambient conditions (humidity, temperature, etc.) during manufacturing and also by void content and fiber volume/weight fraction in the composite. Chen *et al* [26] investigated the effect of fiber volume fraction on the fracture toughness values calculated by different fracture toughness calculation methods using data obtained through mode I testing. They observed that the fracture toughness values $G_{Ic}(NL)$ (toughness values obtained by considering load and deflection values at the point where load-displacement curve deviates from linear response) and $G_{Ic}(Prop)$ (stable crack propagation toughness values) decreased with increasing fiber volume fraction. Other fracture toughness values usually calculated from mode I testing are $G_{Ic}(VIS)$ (fracture

toughness measured by considering load and deflection values at the point on the load-displacement curve corresponding to time when delamination is visually observed) and $G_{Ic}(5\% \text{ max})$ (fracture toughness value corresponding to the point on the load-displacement curve at which the compliance has increased by 5% or the load has reached the maximum value). No general trends were observed for these values with increasing fiber volume fraction for the tested unidirectional glass fiber reinforced polyamide 12 composites.

For a part of the work described in this report, mode I testing was used to compare the relative fracture toughness values $G_{Ic}(NL)$ at crack initiation and $G_{Ic}(Prop)$ during delamination propagation for repairs carried out using different repair resins. $G_{Ic}(NL)$ values are typically lower than $G_{Ic}(VIS)$ and $G_{Ic}(5\% \text{ max})$ and correspond to delamination initiation within the interior of the specimen [18]. $G_{Ic}(Prop)$ values are plotted against delamination length to form a resistance curve (R – curve) in order to characterize propagation of delamination in case of unidirectional fiber composites. Thus, $G_{Ic}(NL)$ and $G_{Ic}(Prop)$ values provide fracture toughness information that can be used to create a delamination failure criterion suited for designing durable and damage tolerant repairs of unidirectional composite laminates.

Fatigue Testing

As composite structures are frequently subjected to cyclic loading, fatigue testing of composite repairs is an important aspect of designing repairs. It provides information about the service life of the repaired composite part. The process of designing and analyzing composite repairs began in Australia about four decades ago [27]. In the United States, the use of composite materials for repairs became prevalent three decades ago [28,

29] when Warner Robins Air Logistics Center and Lockheed Aeronautical Systems Company began applying boron/epoxy repairs to damaged primary metallic parts of airplanes. Since then, a lot of research and testing related to fatigue has been carried out in order to design and standardize composite repairs on aluminum and steel parts [30-45]. For example, Toudeshky *et al* [38] conducted finite element analysis (FEA) on the effects of different glass/epoxy repair lay-ups on cracked aluminum panels with stiffeners by using a previously developed finite element method (FEM) macro program to trace crack growth under mode I and mixed mode fatigue loading. Contemporary researchers [41, 43] found that the fatigue life of cracked steel plates repaired with carbon/epoxy patches improved over two times than that of unpatched plates. In a different study [45], two aluminum alloy 5052-H32 parts were adhesively bonded at different angles to form a dog bone specimen and tested under tension – tension fatigue in order to establish a relationship between fatigue life and scarf angle in case of adhesively bonded scarf repairs.

With the gradual transition from a complete metal to a complete composite fuselage in aircrafts, and due to the increased use of FRP composites in the defense, transport, energy and recreational sectors, the focus on improving composite repairs on FRP composite parts has increased over the past few years. Most of the research on fatigue behavior of bonded composites has been confined to that involving composite parts joined together by adhesives like epoxy [46-50]. Bernasconi *et al* [46] tested, under mode I fatigue loading, DCB specimens with adherends made of carbon/epoxy pre-preg parts and glued together by a two-part epoxy system. The data obtained was used to characterize tension-tension fatigue crack propagation along the bondline of two composite parts adhesively

bonded together in a single lap joint. In both cases, the cracks initiated within the adhesive at starting points of the joints and then propagated into the plies adjacent to the adhesive bondline. Mattos *et al* [47] conducted a similar study to propose a damage model for single lap joint adhesively bonded composite specimens. Autoclave molded carbon/epoxy composite parts were bonded together with a two part epoxy adhesive and tested under tension – tension fatigue to establish a relationship between the overlap length and strength of the composite joint. In a series of studies [48-50], Fernandez *et al* characterized fatigue behavior of adhesively bonded composite joints under mode I, mode II and mixed mode I – mode II loading respectively. In the first case, DCB specimens were tested under mode I fatigue loading and a data reduction technique was proposed in order to get rid of the cumbersome and difficult process of monitoring crack growth propagation during testing. This data reduction technique based on specimen compliance and beam theory was later used to characterize composite bonded joints under fatigue End Notched Flexure (ENF) and Single-Leg Bending (SLB) tests for mode II and mixed mode I – mode II loads respectively.

A considerable amount of research has been conducted on fatigue characterization of initially undamaged fiber reinforced composites [51 – 59], composite repairs on metal parts and adhesively bonded pre-formed composite parts. There is little published material related to fatigue analysis carried out on composites repaired with fiber reinforced composites using hand lay-up or other composite manufacturing techniques such as vacuum assisted resin transfer molding (VARTM), resin transfer molding (RTM) or autoclave manufacturing. However, there have been very recent studies such as by Caminero *et al* [60] involving static testing and health monitoring of fiber reinforced

composite scarf repairs using Lamb waves and modern techniques like 3-D digital image correlation. The second part of the work conducted for this treatise involves tension – tension fatigue testing carried out to finalize a new repair resin candidate out of those selected from screening by mode I testing.

Mixed-Mode (Mode I & II) Testing

Under realistic conditions, delamination in fiber reinforced composite structures may be due to a combination of mode I and mode II loads. Thus, it is necessary to test repairs carried out on composite parts under mixed mode I – mode II loading. In 2001, ASTM International developed the Standard Test Method for Mixed Mode I – Mode II Interlaminar Fracture Toughness of Unidirectional Fiber Reinforced Polymer Matrix Composites (ASTM D 6671/D 6671M – 06) [61] for evaluating the interlaminar fracture toughness of unidirectional fiber reinforced polymer matrix composites under mixed mode I – mode II loading. Though this method describes in detail the mixed-mode bending (MMB) test as applicable to use with unidirectional carbon fiber tape laminates [62-65] with brittle and tough single-phase polymer matrices, it has also been extensively used to test the toughness of both glass fiber reinforced composites and materials bonded with adhesive joints [66-72]. This test method is based on the criterion suggested by Benzeggagh *et al* [66] to represent the mode I and mode II interaction envelope. They also established that the MMB test allows the generation of the R – curve for delamination of fiber composites tested under any mode I – mode II ratio loading. In an initial study, Ducept *et al* [67] successfully established the reliability of the beam theory analysis of the MMB test and its applicability to test low modulus unidirectional glass fiber reinforced composites similar to those obtained by hand lay-up repairs. They also

found that the $G_{Ic}(NL)$ crack initiation values obtained at insert tip are independent of the thickness of the specimens. On the other hand, $G_{Ic}(5\% \text{ max})$ values depend strongly on specimen geometry and lower mode II fracture toughness values are obtained in this case. They then validated that the beam theory and experimental compliance MMB partitioning methods predict the same mixed mode ratios [68]. Compliances for the partitioning methods were measured from DCB and ENF tests. The above mentioned validations for the MMB test were then applied to test adhesively bonded glass/epoxy composite joints and it was found that fracture toughness values for these are much higher [69] than those obtained from delamination of unidirectional glass fiber reinforced epoxy composites. Also, mixed mode I – mode II delamination of unidirectional glass/epoxy composites manufactured by hand lay-up follows linear elastic fracture mechanics (LEFM). The use of MMB test for low modulus fiber glass composites was further validated by Dharamawan *et al* [70] when they tested glass/vinylester composites used for marine applications. The limiting criteria were that the load opening displacement should not be large enough so as to violate the use of LEFM and that the specimen arms should not get damaged. ASTM International is still in the process of developing a method for characterizing delamination of composites under mode III loading. Round robin testing has been carried out using modifications of the edge crack torsion (ECT) method which was initially proposed by Lee [73]. Mendes *et al* [71] tested unidirectional glass/epoxy pre-preg composite specimens using DCB, ENF, MMB and ECT tests and fitted the results with numerical simulation of delamination under various modes. They verified that a 3D modification [74] of the mode I – mode II criterion suggested by Benzeggagh *et al* is applicable to delamination of composites under mixed

mode II – mode III and mixed mode I – mode III loading. Recent work by Blake *et al* [72] suggests successful applicability of the MMB test to heavily woven glass fabric composites with a rubber toughened vinyl ester polymer matrix. They observed that the crack growth was dependent on the type of weave but the fracture toughness characteristics and R – curves are similar to those as found with unidirectional glass fiber composites. For last part of the current work, mixed mode I – mode II testing was used to characterize glass fiber/polymer composite repairs conducted using hand lay-up technique on parent parts manufactured by vacuum assisted resin transfer molding (VARTM). Differences in some repair parameters were investigated.

As mentioned above, a lot of research has been conducted on repairs of composite structures with critical and high value applications such as those in aerospace. There is very little literature available that pertains to repair of fiberglass/polymer composite structures that are being produced worldwide on a massive scale for marine, transport, energy and civil engineering infrastructure, etc. These industries are on a constant search for better repair possibilities in order to cut down their manufacturing cycle times and repair costs. Repairs may be required as a part of the manufacturing process or due to damage while in service. Such repairs, usually wet patch or scarf, are conducted in situ by hand layup techniques. The scope of this study is the mechanical component of an effort to enhance the performance of wet hand layup repairs for a wind turbine blade manufacturing company which also sponsored this work. Mechanical properties of hand layup repairs conducted with different repair resins and repair parameters were investigated under mode I, tension – tension fatigue and mixed – mode I mode II loading.

CHAPTER II

EVALUATION OF GFRP REPAIRS BY MODE I TESTING

Introduction

This chapter contains details of mechanical testing of Double Cantilever Beam (DCB) composite specimens comprising a Vacuum Assisted Resin Transfer Molding (VARTM) infused parent plate and a hand laid-up upper plate simulating a typical blade repair. The testing was carried out as part of an effort to optimize a new repair resin for a wind turbine blade manufacturing company. To increase repair performance and in order to identify an optimum repair resin, many resin vendors were contacted for the current work. From more than fifteen candidate resins, nine resins were chosen for initial screening. After studying the literature obtained with these resins and information acquired from their respective vendors, six resins were found to suit the requirements of the sponsoring company. Unidirectional glass fibers and a polymer resin are currently used to manufacture the company's blades. Because delamination of the repair from the parent blade is a major concern, the testing method detailed in ASTM D 5528 (Test Method for Mode I Interlaminar Fracture Toughness of Unidirectional Fiber-Reinforced Polymer Matrix Composites) [18] was followed to determine fracture toughness values of the prospective repair resin candidates.

Resin Selection

Resin additives such as rubber and styrene have a considerable effect on the mechanical properties of FRP composites. Diffusion of styrene from the repair resin into pre-cured resin of the parent plate can lead to stronger bonding of the repair resin with the parent plate [75]. Rubber additives increase ductility of the repair resin and thereby the fracture toughness of the repair [76]. The six repair resins chosen had varying formulations with different quantities of rubber and styrene. The compositions are given in Table 2.1.

Table 2.1. Compositions of repair resins.

Resin	MB-B	NRR1	NRR2	NRR3	NRR4	NRR5	NRR6
Resin Type	Polyester + Styrene	Vinyl ester + Styrene + Rubber additives	Vinyl ester + Styrene	Vinyl ester + Low styrene	Vinyl ester + High styrene	Vinyl ester + Core shell rubber (100 nm)	Vinyl ester + Core shell rubber (200 nm)

Specimen Fabrication

For repair resin screening, DCB specimens (Figure 2.1) were manufactured in accordance with ASTM D 5528 and consisted of two separate parts: the lower adherend or parent plate, representing the blade, and the upper adherend or repair plate, simulating the flat part of a one-sided scarf repair. Both adherends consisted of an even number of plies. A description of the lay-up and the materials used is given in Table 2.2. The company uses a different polyester resin (MB-B) for repairs currently than is used to fabricate the shell of the blade (MB-A). The parent plates for the DCB specimens were made using the current blade shell resin. Simulated repairs were fabricated using each candidate repair resin. Simulated repairs using the current repair resin (MB-B) were tested to serve as a baseline for comparison.

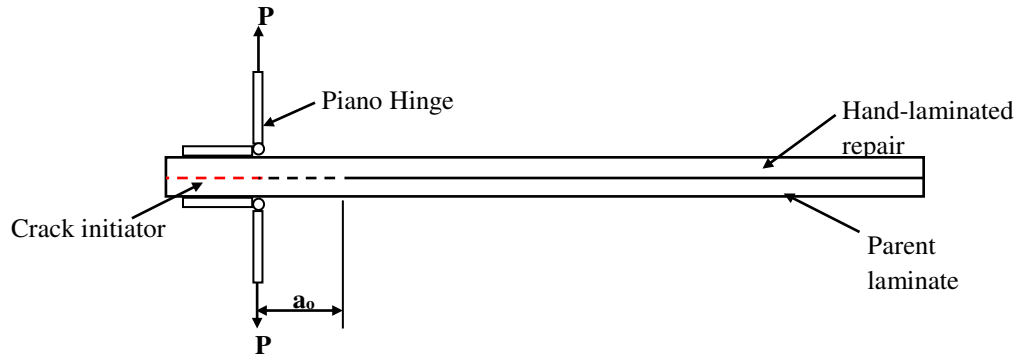


Figure 2.1. DCB Specimen

Table 2.2. Mode I test specimen lay-up, materials used and curing details

Lay-up (top to bottom)	Part	Details
2 x Biaxial plies ($\pm 45^\circ$)	Repaired Laminate: Hand Lay-up Repair Resin (Upper adherend)	Curing: 24 hrs. at room temperature Post curing: 16 hrs. at 40°C
8 x Unidirectional plies (0° with CSM – CSM facing downwards)		
Chopped strand mat (CSM)		
Insert (Crack Initiator)	Polymer film	Thickness $\leq 13\ \mu\text{m}$
8 x Unidirectional plies (0° with CSM – CSM facing downwards)	Parent Laminate: VARTM Main Blade Resin (Lower adherend)	Curing: 24 hrs. at room temperature Post curing: 24 hrs. at 60°C 3 hrs. at 95°C
2 x Biaxial plies ($\pm 45^\circ$)		

The parent plate representing the blade was manufactured using Vacuum Assisted Resin Transfer Molding (VARTM). A VARTM setup, before vacuum bagging and infusion of resin, is shown in Figure 2.2. After the gelling of the resin, the parent plates were cured at room temperature for 24 hours, and then further post-cured at 60°C for 24 hours and then at 95°C for 3 hours. This was done to fully cure the parent plates and also to have low residual styrene content by minimizing incomplete polymerization through high curing temperature. All parent plates were made continuously one after the other and each plate was then assigned to a repair resin candidate. Care was taken that the time lapse between

manufacture of a parent plate and conducting repair on it was almost the same for each case.



Figure 2.2. VARTM set-up before infusion

Each parent plate initially consisted of nine, 0.88 mm thick plies with unidirectional glass fibers and a chopped strand mat attached on one side (called Combi plies hereafter) and two biaxial plies (plies with glass fibers at $\pm 45^\circ$) at the bottom (Figure 2.3). Since the lay-up of the parent plate was not symmetric, some warp was observed in the parent plates perpendicular to the direction of the unidirectional fibers in the Combi plies. The extent of warp is depicted in Figures 2.4 and 2.5. The reading on the scale (depth of warp) in Figure 2.4 is 1.25 cm. The total width of the plate was 60 cm. As the specimens were to be cut along 1-direction (direction along fibers), it was decided that the warp would not have a significant effect on the test results.

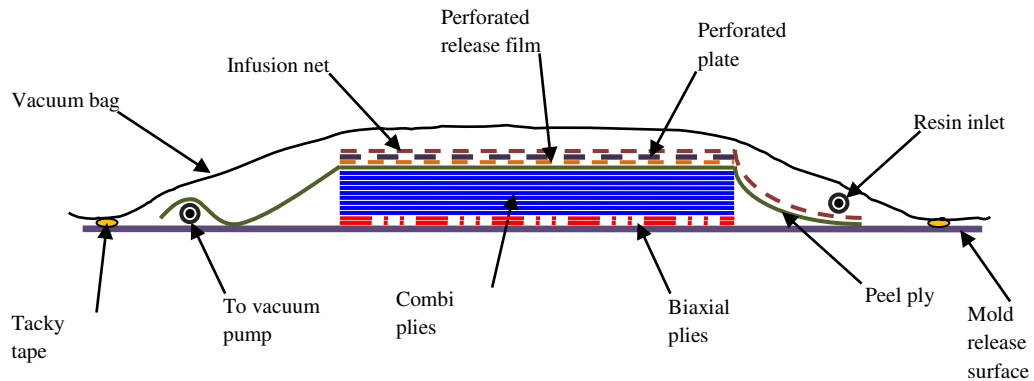


Figure 2.3. VARTM infusion package



Figure 2.4. Straight rule along Combi plies' 0° direction (1 – direction)



Figure 2.5. Straight rule along Combi plies' 90° direction

Following post-curing of the parent plate, the top layer was completely ground off, resulting in an exposed layer of resin to serve as the repair surface. This exposed surface of the parent plate was first scrubbed with the repair resin using a hard brush and then the simulated repair, consisting of eight Combi plies, a chopped glass strand mat (CSM) and a polymer insert in the sequence given in Table 2.2, was applied by hand lay-up. The hand lay-up comprised of applying the repair resin with the help of a soft roller and then using a hard roller to smooth the plies and remove trapped air bubbles, if any. The repairs were then covered with peel ply and left to cure at room temperature. After a cure of 24 hours at room temperature, the whole sample was then post – cured at 40°C for 16 hours. Certain parameters such as the gel time, peak exothermal temperature, time to peak exotherm and ambient conditions were recorded (Table 2.3) to facilitate calculations for the degree of cure of the new repair resin candidates. This was done to compare resin behavior during the actual manufacturing process with their behavior during laboratory testing of pure resin using rheology and differential scanning calorimetry. In order to

obtain a specific desired quality of laminates, the post – curing conditions for resins having different compositions are not the same. Shore D hardness values were noted before and after post curing to verify that post curing at the above mentioned temperatures and time duration did not have any adverse effects on the quality of the repair adherends. The plates were then cut with a diamond saw to procure specimens nominally 35 cm length and 3 cm wide.

Table 2.3. Recorded values for new repair resins.

Resin	MB-B	NRR1	NRR2	NRR3	NRR4	NRR5	NRR6
Gel time (min.)	66	52	60	62	120	120	65
Peak exothermal temperature (°C)	38.4	35.4	45.0	35.4	30.2	36.6	53.4
Peak time (min.)	172	147	103	159	300	176	107
ShoreD hardness before post-curing (mean of 10 values)	87.8 ± 1.0	86.4 ± 1.5	87.5 ± 1.5	87.9 ± 1.0	88.5 ± 1.0	86.6 ± 1.5	85.7 ± 1.5
ShoreD hardness after post-curing (mean of 10 values)	88.1 ± 0.5	86.8 ± 1.0	88.0 ± 1.0	88.0 ± 0.5	88.8 ± 1.5	88.0 ± 1.5	86.2 ± 1.5
Room Temperature (°C)	21.0	21.0	21.5	21.0	21.0	21.7	21.7
% R. H.	44.0	15.0	11.5	44.0	15.0	12.0	12.0
Initiator Type	MEKP	MEKP	MEKP	MEKP	MEKP	MEKP	CHP - MEKP
Fiber volume fraction (± 2.5%)	56.2	60.0	58.3	59.6	60.6	59.0	55.0

A polymer insert with a thickness less than 13µm was used to create a pre-crack of approximately 30 mm at the resin inlet side during the simulated repair. Piano hinges were glued with Araldite® to the surfaces of the cut specimens to facilitate pulling apart of the two adherends. The areas of the specimen surfaces where the hinges were to be glued were sanded lightly to get a strong bond between Araldite® and the composite

surface. The final DCB specimen dimensions were 350 mm in length and 30 mm in width. The parent laminate adherend had a thickness of 7.7 ± 0.3 mm whereas the repair laminate was 10.2 ± 0.7 mm thick. Both edges of the specimens were coated with a water-based white typewriter fluid and thin lines were marked every 1 mm on either edge for a distance of 100 mm from the end point of the pre-crack. The coating and markings were added to aid in the observation of crack propagation during testing. To compare the toughness of the repairs with that of the main blade, a batch of DCB specimens was made in which the main blade resin (MB-A) was used for both adherends. These specimens were manufactured with both adherends together under vacuum using VARTM followed by a room temperature cure for 24 hours, a post-cure at 60°C for 24 hours, and then a final cure at 95°C for 3 hours. The lay-up was the same as that of the DCB specimens made with repair resin candidates and the adherends had a thickness of 8.35 ± 0.04 mm.

Testing

Testing of the DCB specimens was conducted on the Shimadzu AG-IS Universal Testing Machine under displacement control at a crosshead rate of 0.1 mm/min. Higher rates were tried but at those rates crack propagation was too fast for collection of adequate data for fracture toughness calculations. The specimens were aligned and centered with the help of a level when the hinges were being mounted in the load grips with the parent laminate down as shown in Figure 2.6. The end of each specimen, opposite to the end where the hinges were attached, was supported before loading. It was noticed that the supported end lifted (less than 1.0 mm) off the support as the load was applied. Crack propagation was monitored and recorded with the help of a Retiga 1300 camera (Figure 2.6).



Figure 2.6. Experimental set-up for DCB testing

Load data was recorded using TRAPEZIUM 2 control software linked to the universal testing machine and images of the loaded samples were captured and analyzed for displacements using Vic-Snap digital image and Vic 2D correlation software respectively. Initially, testing was conducted with the adherends of the specimen being pulled apart continuously. It was noticed that the crack growth was primarily run-arrest extension in which the delamination front jumped ahead abruptly rather than being a slow, stable extension [18]. In order to be able to monitor crack growth effectively, following each 15 mm crack growth increment, the load was reduced by 30% and then the specimens were reloaded to continue the test; this procedure was repeated at least five times for each specimen. In order to procure statistically significant data, five specimens were tested for each of the resin samples.

Calculations

The mode I critical strain energy release rate (interlaminar fracture toughness, G_{Ic}) for a built-in double cantilever beam can be calculated by using the load data obtained from

each sample, along with values for the opening displacement according to ASTM D5528 as

$$G_{Ic} = \frac{3P\delta}{2ba} \quad (2.1)$$

where P = applied load, N, δ = load point deflection, mm, b = width of DCB specimen, mm, and a = delamination length, mm. This expression is expected to overestimate the actual value of the material property due to incorrect boundary conditions. A corrected value, G_{Ic}' , can be calculated [18] as

$$G_{Ic}' = \frac{3P\delta}{2b(a+|\Delta|)} \quad (2.2)$$

where Δ corrects for beam rotation at the delamination front. The correction factor, Δ , is obtained from the least squares fit of a plot of the cube root of compliance of the DCB specimen as a function of the delamination length. The compliance of the beam can be calculated as the beam deflection at the point of applied load divided by the applied load, δ/P . This is a decreasing function of the crack length, a , measured from the point of applied load to the crack tip. Since the ratio of load point displacement to initial crack length, δ/a_0 , did not exceed 0.4, large deflection corrections were not required. It should be noted that ASTM D5528 does not strictly apply to this test geometry. Despite the similar layup between the parent plate and the simulated repair, the hand lay-up process produces a significantly thicker top portion of the final plate. The ratio of the parent plate thickness to the hand-layup thickness, h_1/h_2 , is approximately 0.75 (averaged value). As a result, the DCB specimens are not symmetric about the crack plane. This is in addition to a slightly non-symmetric fiber lay-up. Specimen asymmetry leads to the presence of mode II (shear) loading at the crack front which is not present in a symmetric DCB

specimen. Multiple approaches for calculating the overall strain energy release rate, G , and the mode I and mode II components, G_I and G_{II} , exist [68, 77-80]. For example, the method of Hutchinson and Suo [80] requires that the applied loading on the specimen be separated into several component moments. This requires either a modification to the experimental setup to measure additional loads or the use of complimentary numerical calculations. However, Mollón and co-workers [77] present a relationship to calculate the mode mixity that they found to work well over a range of material properties, Equations 2.3 – 2.6.

$$\alpha = \frac{1 - \frac{h_1^3}{h_2^3}}{1 + \frac{h_1^3}{h_2^3}} \quad (2.3)$$

$$\beta = 0.06\alpha + 0.35 \quad (2.4)$$

$$\frac{G_{II}}{G} = -\beta\sqrt{1-\alpha^2} + \beta \quad (2.5)$$

$$\frac{G_I}{G} = 1 - \frac{G_{II}}{G} \quad (2.6)$$

Based on this analysis, G_{II}/G is approximately 0.030 ± 0.012 for the geometry tested in this work. Thus, the mode I analysis presented in [18] should lead to an acceptable level of accuracy.

Results and Discussion

The ratios of corrected values of interlaminar fracture toughness, G_{Ic}' , to the fracture toughness value for main blade resin at crack initiation, G_{Ic0}' , were calculated using Equation 2.2 for each increment in every batch of specimens tested and plotted against a, the crack length. Figure 2.7 and Figure 2.8 show the resulting curves for the main blade

resin (MB-A) and the current repair resin (MB-B), respectively.

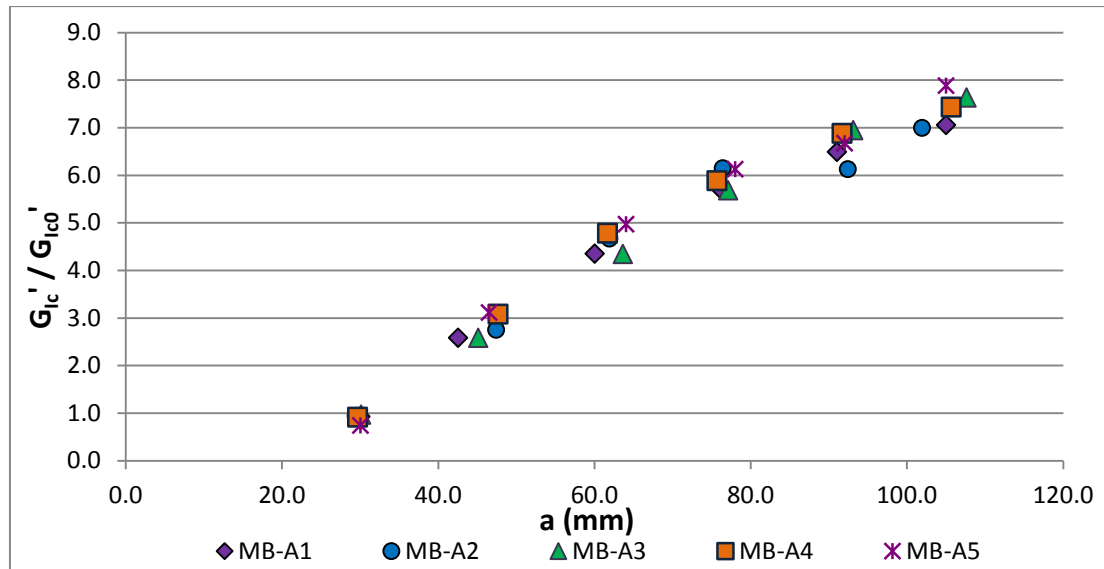


Figure 2.7. G'_{Ic}/G_{Ic0}' vs crack length for main blade resin, MB-A.

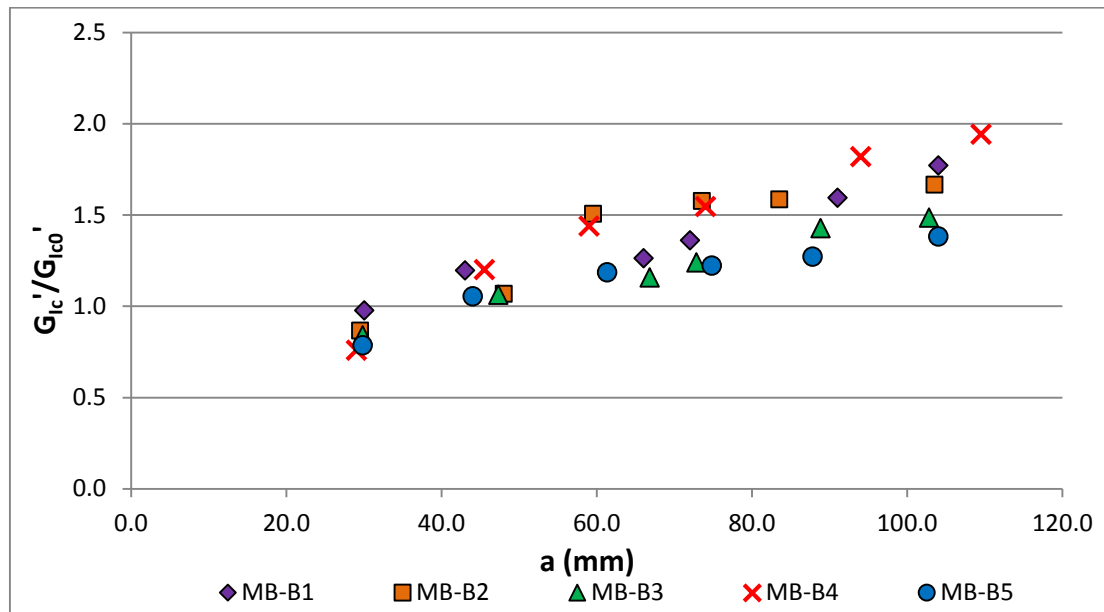


Figure 2.8. G'_{Ic}/G_{Ic0}' vs crack length for current repair resin, MB-B.

These curves indicate the toughness of the main blade at a crack length of approximately 105 mm to be four times more than that of the repairs made by the current repair resin.

On examination of the surfaces of the specimens, it was noticed that, in the case of

specimens made completely with MB-A, the crack propagated through the CSM (Figure 2.9) whereas in the case of the specimens repaired with MB-B, crack propagation was at the interface of the two adherends with the upper adherend (including the CSM) being completely removed from the lower one that represented the blade (adhesive failure). Significant fiber bridging was observed (Figure 2.10) when specimens fabricated completely of the main blade resin (MB-A) were being pulled apart. Little-to-no fiber bridging was observed in specimens made with the currently used repair resin (MB-B). This concurs with post-fracture surface observations. Reduced fiber bridging relative to the main blade specimens was observed during testing of all repair resin candidates. However, several resins exhibited more bridging than the current repair resin. It is evident from the experimental results that there exists a positive correlation between the fracture toughness values and fiber bridging.

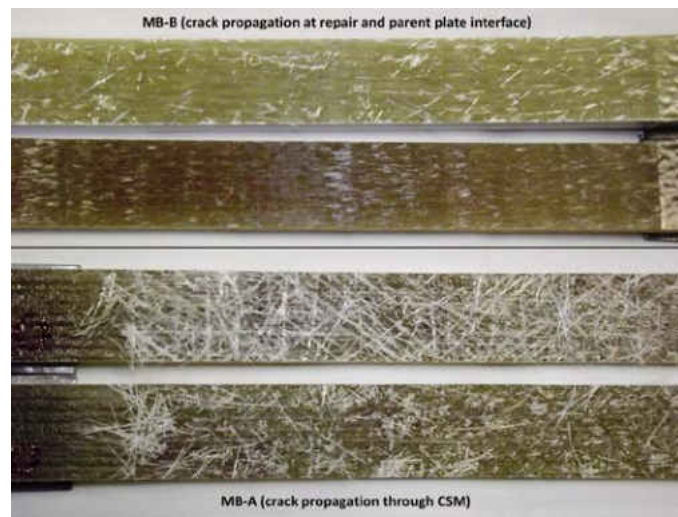
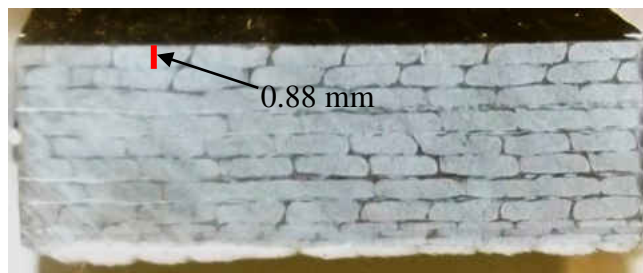


Figure 2.9. Surface morphologies after crack propagation

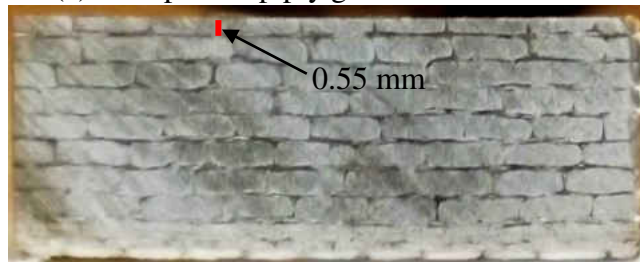


Figure 2.10. Fiber bridging in case of MB-A (main blade resin)

While testing the set of specimens consisting of repairs carried out with repair resins NRR1, NRR4 and NRR5 it was observed that the fracture toughness values obtained were markedly high. Examination of the fractured specimens revealed that the top plies of the parent plates of these specimens had been ground to about half the depth (Figure 2.11) instead of one complete top ply. The specimens for these three resins were manufactured again with the complete top plies ground off so as to get a correct comparison with the other repair resins.



(a) Complete top ply ground off



(b) Partial top ply ground off

Figure 2.11. Grinding difference in case of NRR1, NRR4 and NRR5 resins

G_{Ic}'/G_{Ic0}' values were plotted against crack length for each of the new repair resin (NRR)

candidates (Figures 2.12 to 2.17) to compare with the baseline data obtained from the current repair resin. The profile of almost all the plots was as expected but there was an anomaly in the graph for two specimens of new repair resin candidate three (NRR3) (Figure 2.14). The surfaces of these specimens were examined and patches of dry glass were noticed in the CSM on the repair adherend (Figure 2.18); the positions of these patches corresponded to the spikes in fracture toughness values in the plot. The remaining three specimens also had similar patches though much smaller in size. It was not clear whether the patches were manufacturing defects or due to some property of the resin. However, due to the patches and the erratic nature of fracture toughness values obtained this resin (NRR3) was no longer considered to be a viable candidate even though it gave almost 1.5 times higher fracture toughness values than the current repair resin at crack length of approximately 105 mm.

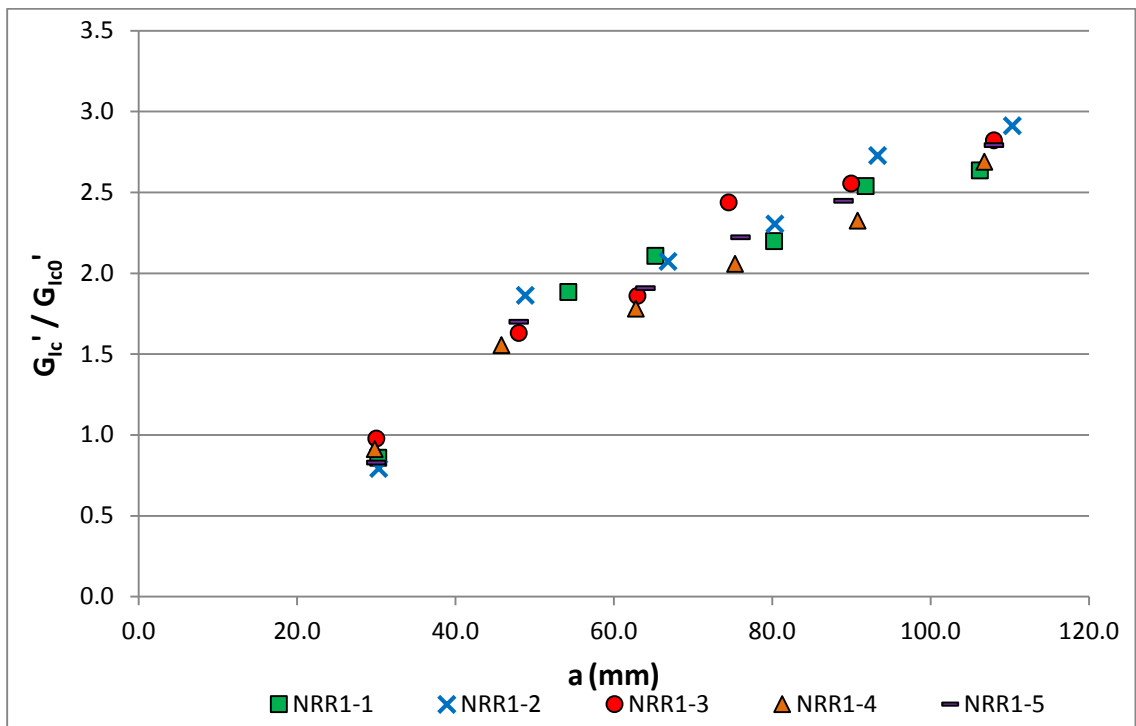


Figure 2.12. G'_{Ic} / G'_{Ic0} vs crack length for candidate resin, NRR1

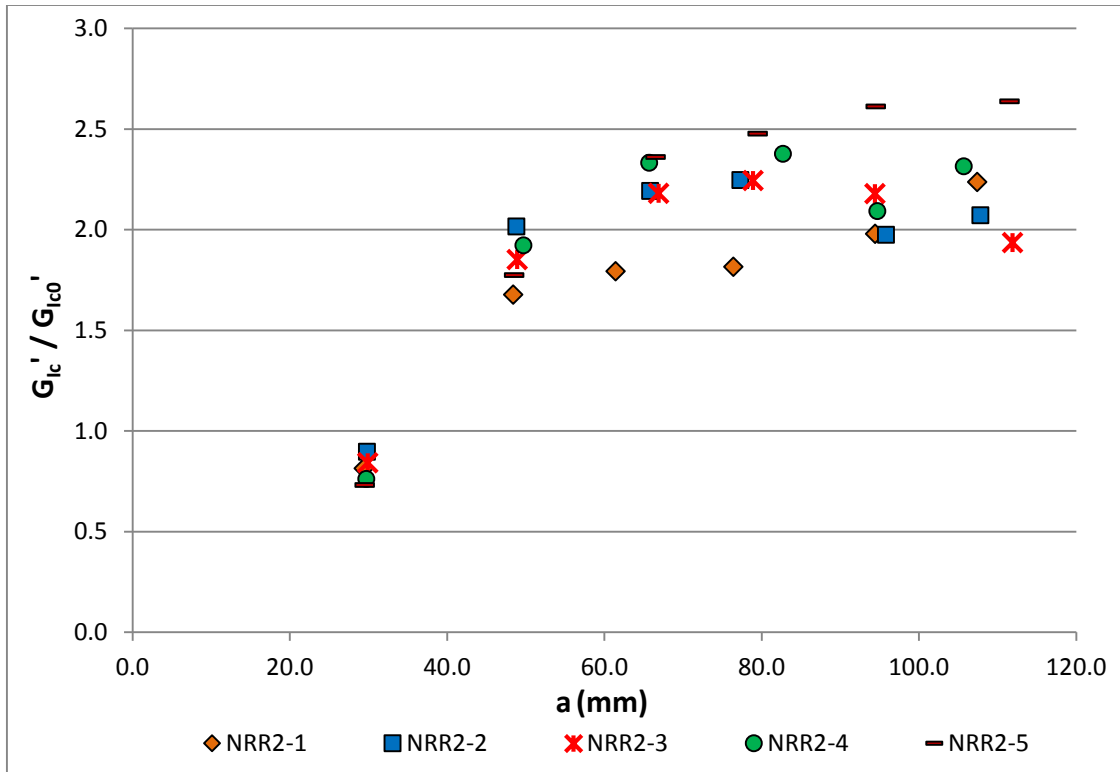


Figure 2.13. G'_{ic}/G'_{ic0} vs crack length for candidate resin, NRR2

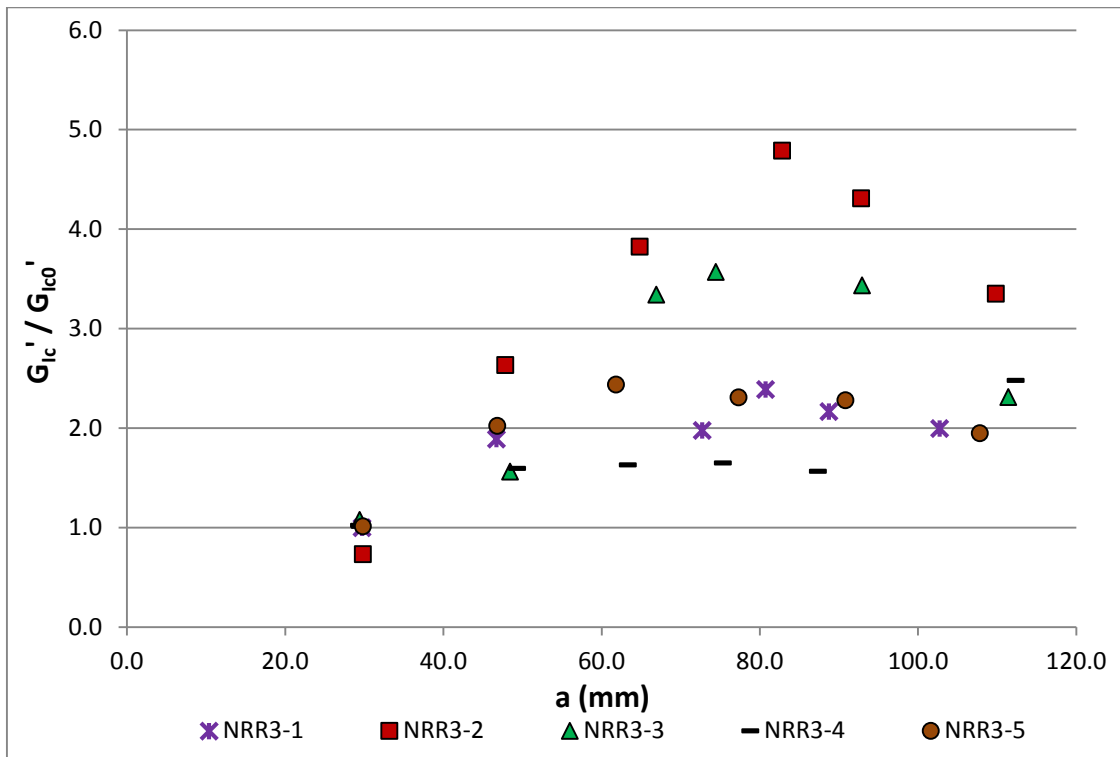


Figure 2.14. G'_{ic}/G'_{ic0} vs crack length for candidate resin, NRR3

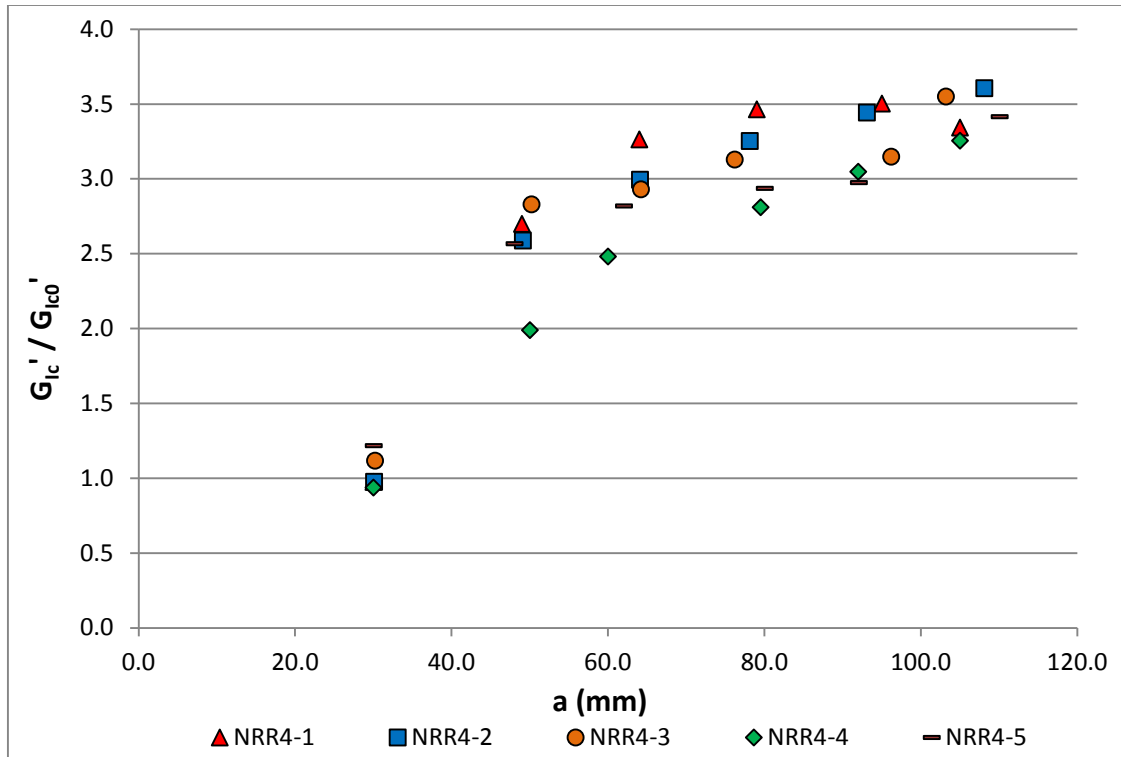


Figure 2.15. G'_{ic}'/G'_{ic0}' vs crack length for candidate resin, NRR4

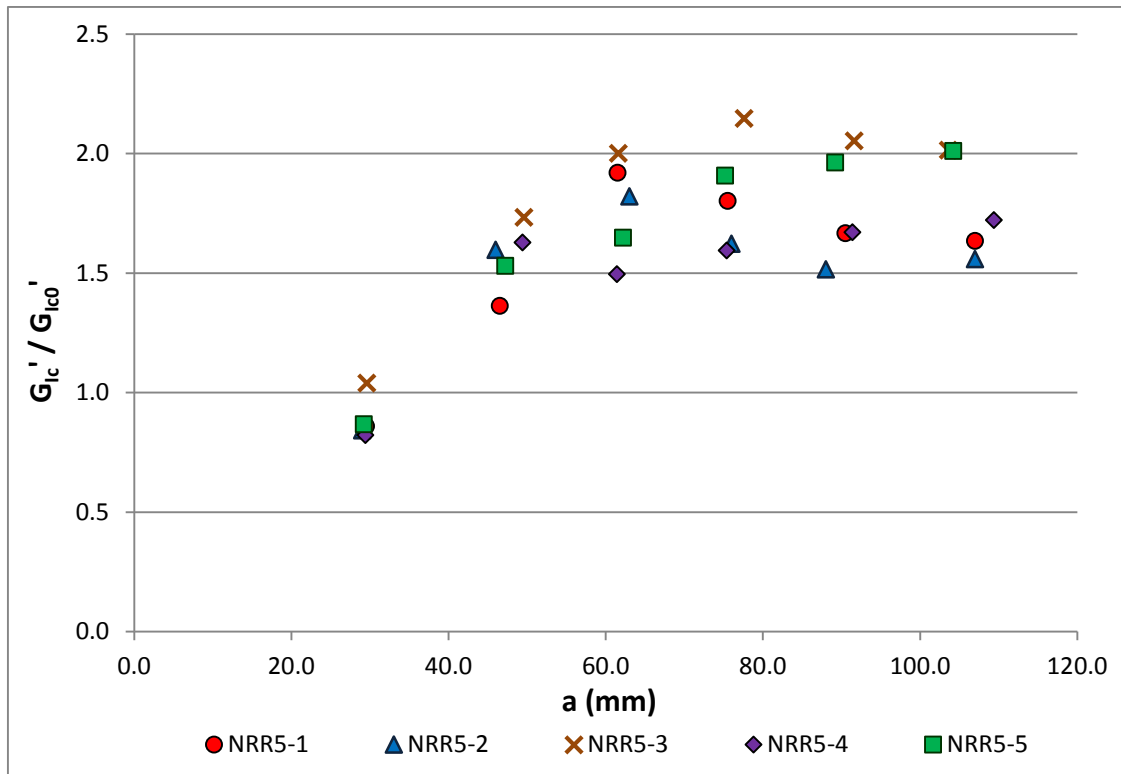


Figure 2.16. G'_{ic}'/G'_{ic0}' vs crack length for candidate resin, NRR5

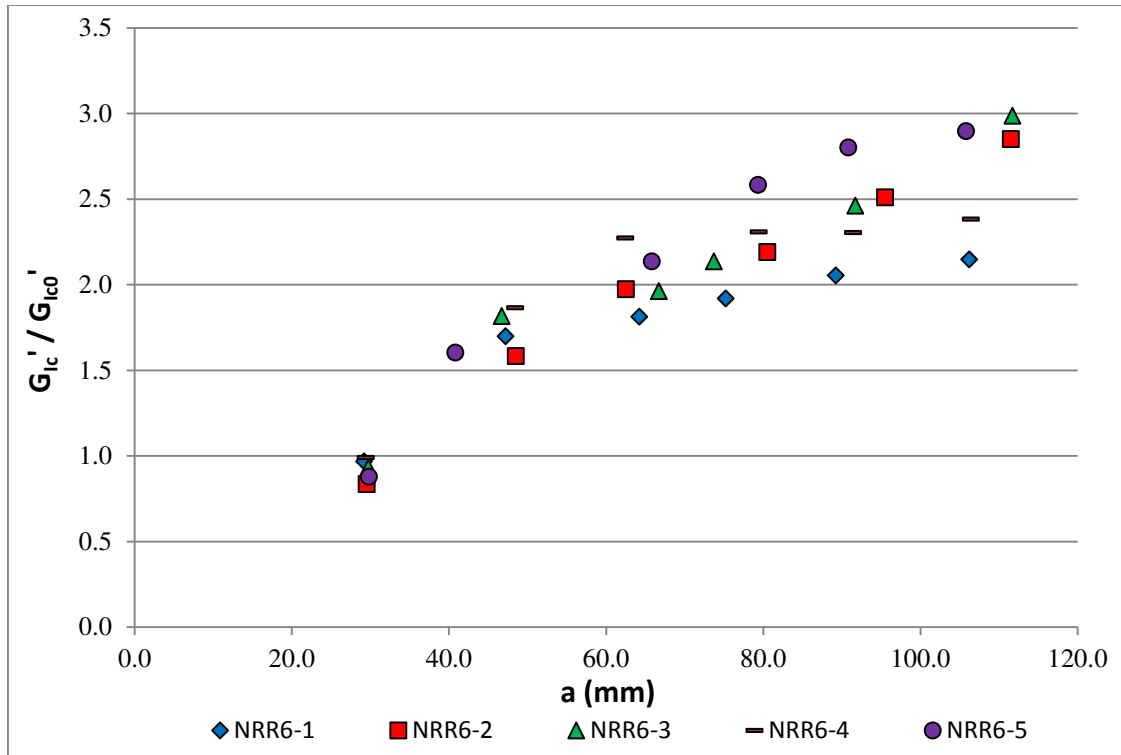


Figure 2.17. G'_{ic} / G'_{ic0} vs crack length for candidate resin, NRR6

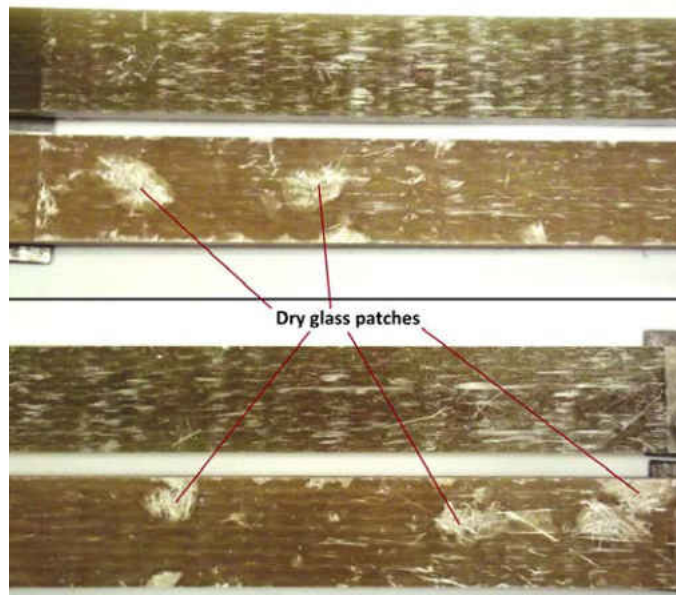


Figure 2.18. Fractured surfaces of NRR3 specimens with dry patches in CSM

Of the remaining five repair resin candidates, three resins (NRR1, NRR4 and NRR6) were identified as the top contenders for the new repair resin. These repair resins had

rubber additives and/or high styrene content which improved their fracture toughness. Out of these, NRR4 had twice the fracture toughness compared to MB-B (Table 2.4) and half the fracture toughness value compared to MB-A at a crack length of approximately 105 mm. Fracture toughness values obtained from NRR1 and NRR6 were respectively 1.6 and 1.5 times those obtained from MB-B. Though the formulation for repair resin NRR5 included core shell rubber particles, it had lower fracture toughness values. While conducting the hand lay-up repair with NRR5 it was noticed that there was foam formation when the methyl ethyl ketone peroxide (MEKP) initiator was mixed in it. After testing, it was visually confirmed that there were voids in the repair adherends of NRR5 specimens. As seen in [81, 82] presence of voids does have an adverse effect on polymer fracture toughness. Thus, repair resin NRR6 was mixed with a blend of cumene hydroperoxide – MEKP (CHP – MEKP) instead of MEKP initiator to avoid foam formation.

Table 2.4. Consolidated mode I fracture testing results (top ply ground off completely)

Resin	MB-A	MB-B	NRR1	NRR2	NRR3	NRR4	NRR5	NRR6
G_{Ic}'/G_{Ic0}' at a ~ 105 mm	7.5 ± 0.5	1.7 ± 0.3	2.8 ± 0.2	2.3 ± 0.3	2.5 ± 0.8	3.4 ± 0.2	1.8 ± 0.2	2.5 ± 0.4
$G_{Ic}'_{NRR}/G_{Ic}'_{MB-B}$			1.6	1.3	1.5	2.0	1.0	1.5

Grinding Variation Study

The specimens with the top plies partially ground off and repaired with repair resins NRR1, NRR4 and NRR5 were also tested to examine the fracture toughness difference due to grinding variation. The normalized fracture toughness values for these are plotted against crack length in Figure 2.19 to Figure 2.21.

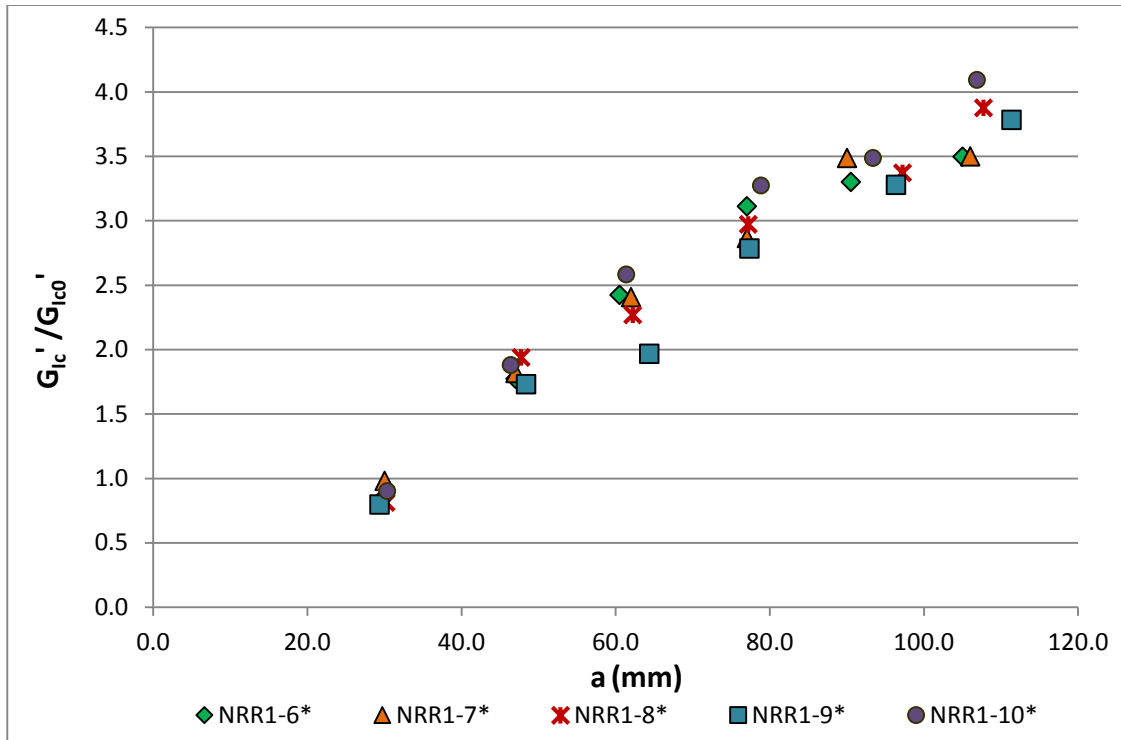


Figure 2.19. G'_{Ic} / G_{Ic0}' vs crack length for resin NRR1 with partial top ply ground off

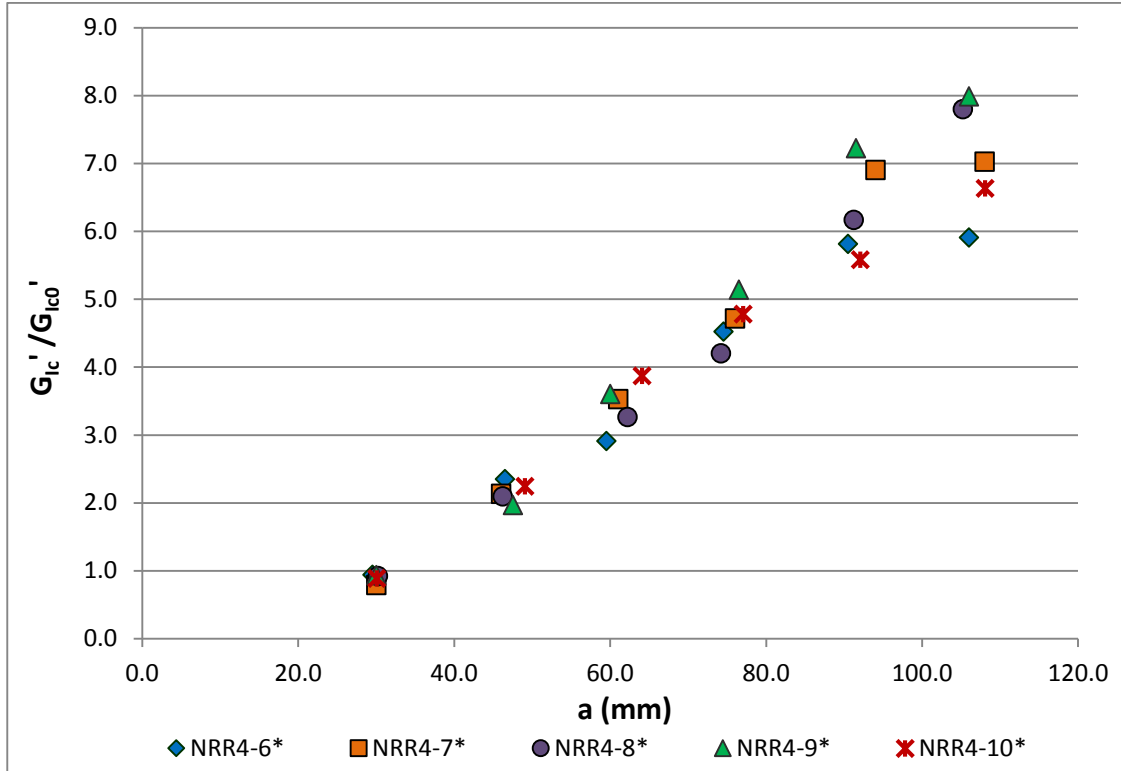


Figure 2.20. G'_{Ic} / G_{Ic0}' vs crack length for resin NRR4 with partial top ply ground off

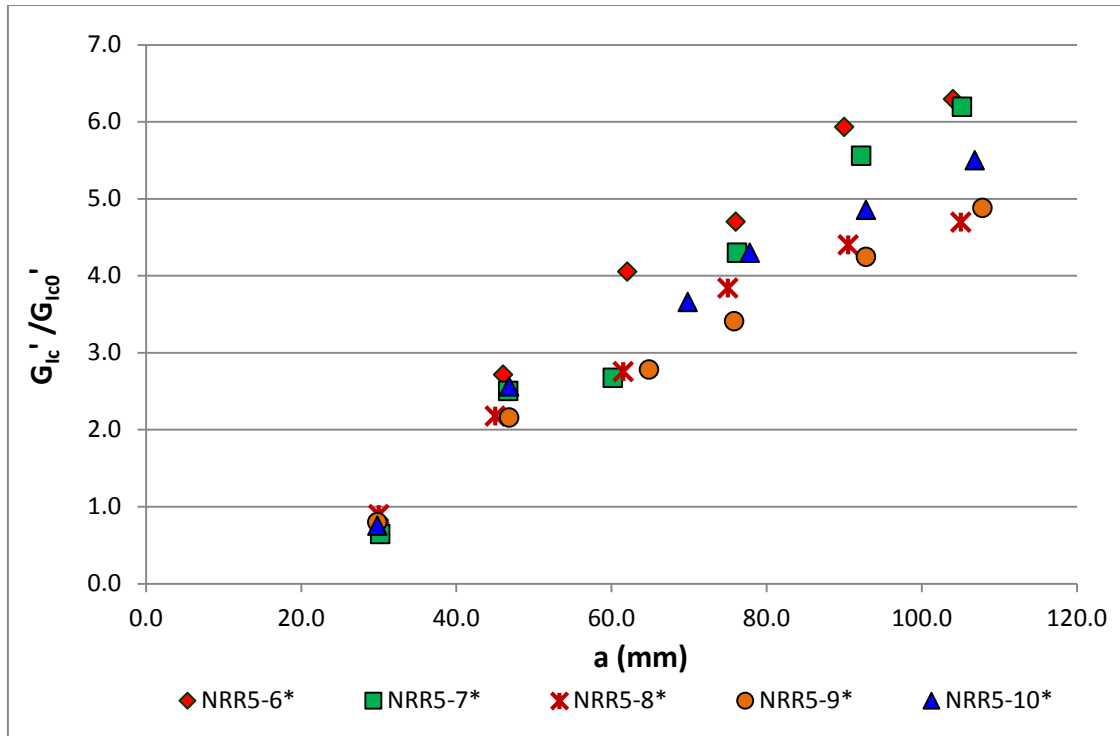


Figure 2.21. G'_{Ic}/G_{Ic0}' vs crack length for resin NRR5 with partial top ply ground off

In all of the specimens with the top plies partially ground off the fracture toughness values were much higher (Table 2.5) than those obtained from specimens made with same repair resins but with their top plies ground off completely. When the top plies are ground off completely, the resulting exposed surface on which the repairs are carried out comprises mainly main blade resin, MB-A. Whereas, when the top plies are ground off partially, the resulting surface has a mixture of exposed fibers and resin. These exposed fibers bond with the repair resin and this results in pronounced fiber bridging while the specimens are being tested, thus leading to high fracture toughness values. Figure 22 to Figure 24 depict a comparison of the normalized fracture toughness values obtained from specimens with top parent plies completely ground off (numbered NRR#-#) to those with the top parent plies partially ground off (numbered NRR#-#*).

Table 2.5. Consolidated mode I fracture testing results (top ply ground off partially)

Resin	MB-A	MB-B	NRR1*	NRR4*	NRR5*
G_{Ic}'/G_{Ic0}' at $a \sim 105$ mm	7.5 ± 0.5	1.7 ± 0.3	3.8 ± 0.3	6.9 ± 0.9	5.5 ± 0.8
$G_{Ic}'_{NRR\#*} / G_{Ic}'_{MB-B}$			2.2	4.0	3.2

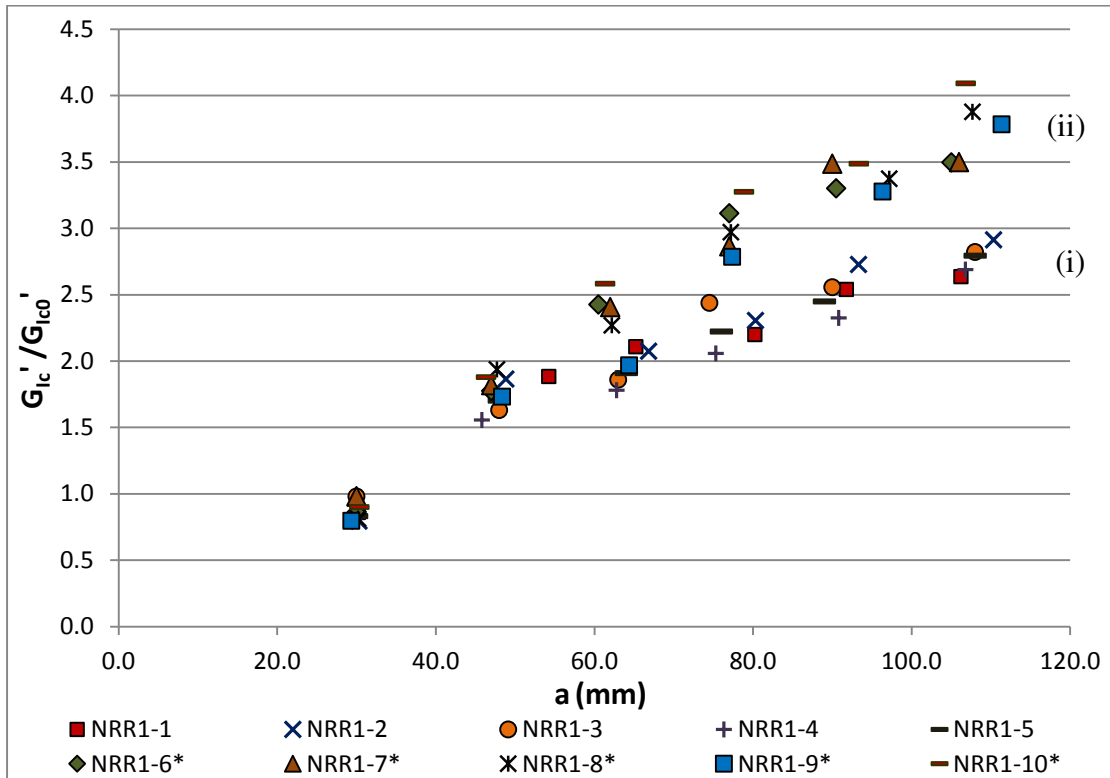


Figure 2.22. Comparison of fracture toughness values of NRR1 specimens with (i) whole top ply ground off (NRR1-#) (ii) partial top ply ground off (NRR1-#*)

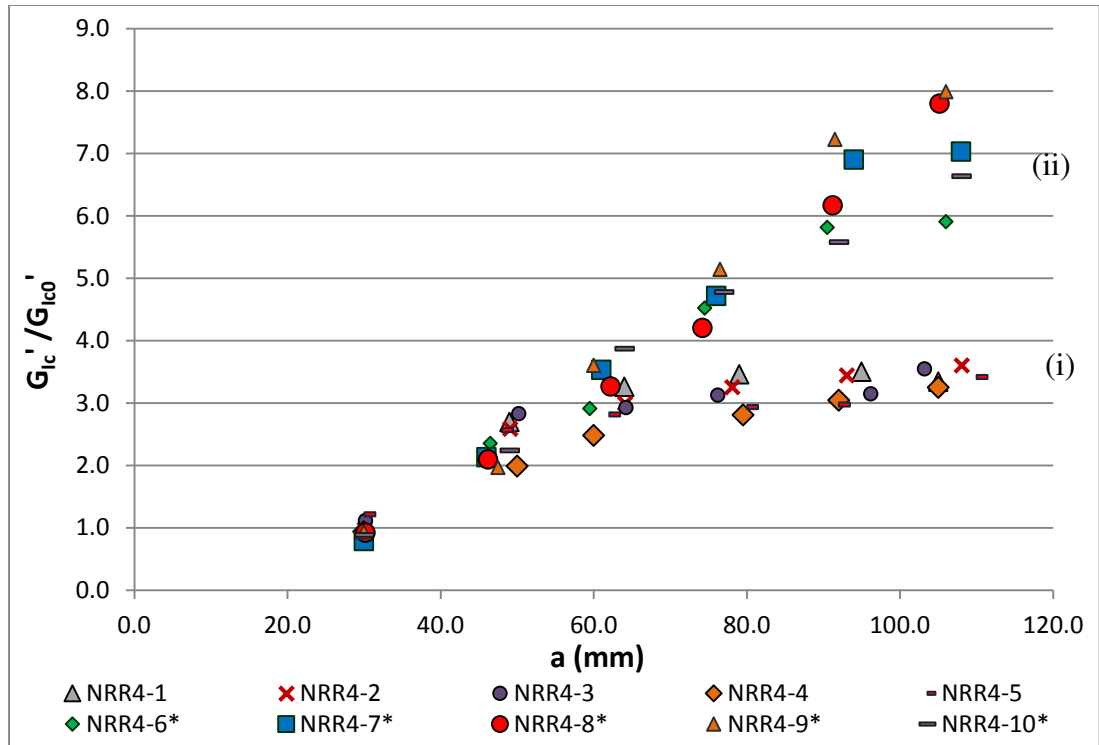


Figure 2.23. Comparison of fracture toughness values of NRR4 specimens with (i) whole top ply ground off (NRR4-#) (ii) partial top ply ground off (NRR4-#*)

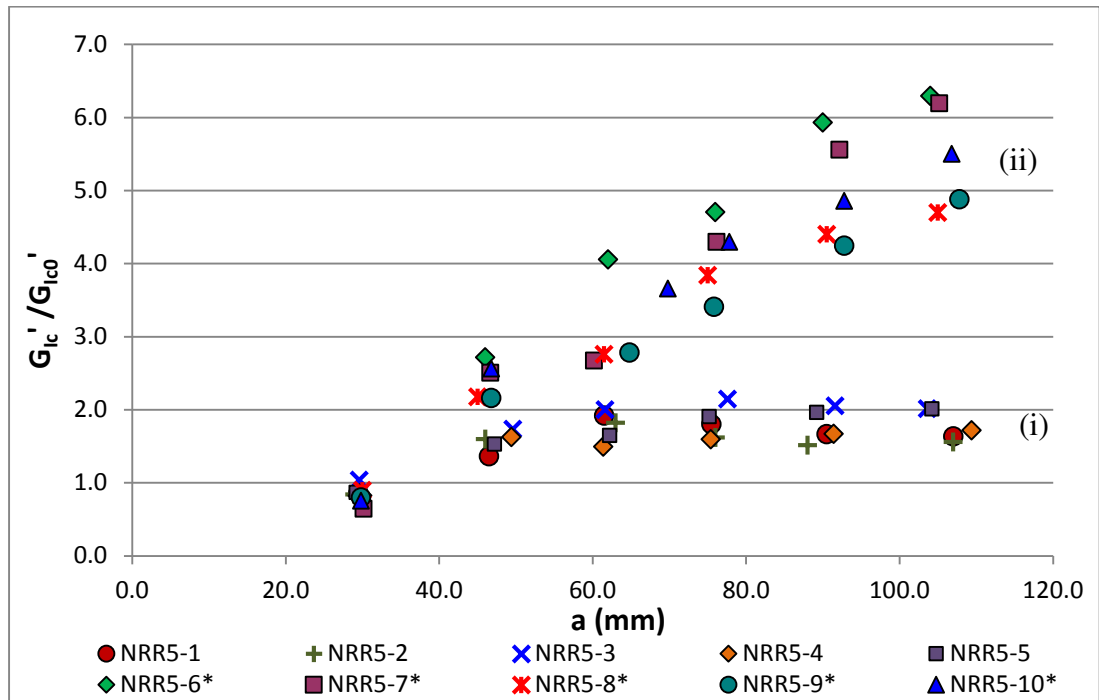


Figure 2.24. Comparison of fracture toughness values of NRR5 specimens with (i) whole top ply ground off (NRR5-#) (ii) partial top ply ground off (NRR5-#*)

From the graphs plotted in Figures 2.22 to 2.24 it is evident that there is little variation in the fracture toughness values at first crack initiation at $a = 30$ mm for the two cases. A closer look reveals that the fracture toughness values, when the specimen first cracks open at the tip of the insert, are higher for the repairs carried out on parent plates with the complete top plies ground off (Figure 2.25). This might be due to the differences in the crack propagation paths in the two cases. For crack initiation at the end of the insert, the fracture toughness values primarily depend upon the bond morphology at the crack tip. The fiber bridging effect comes into play later as the crack propagates along the bondline between the two adherends. In the case of parent plates with the top plies partially ground off the surface at crack tip comprises partial exposed resin and exposed fibers. On the other hand the surface of parent plates with complete top plies ground off comprises mainly resin.

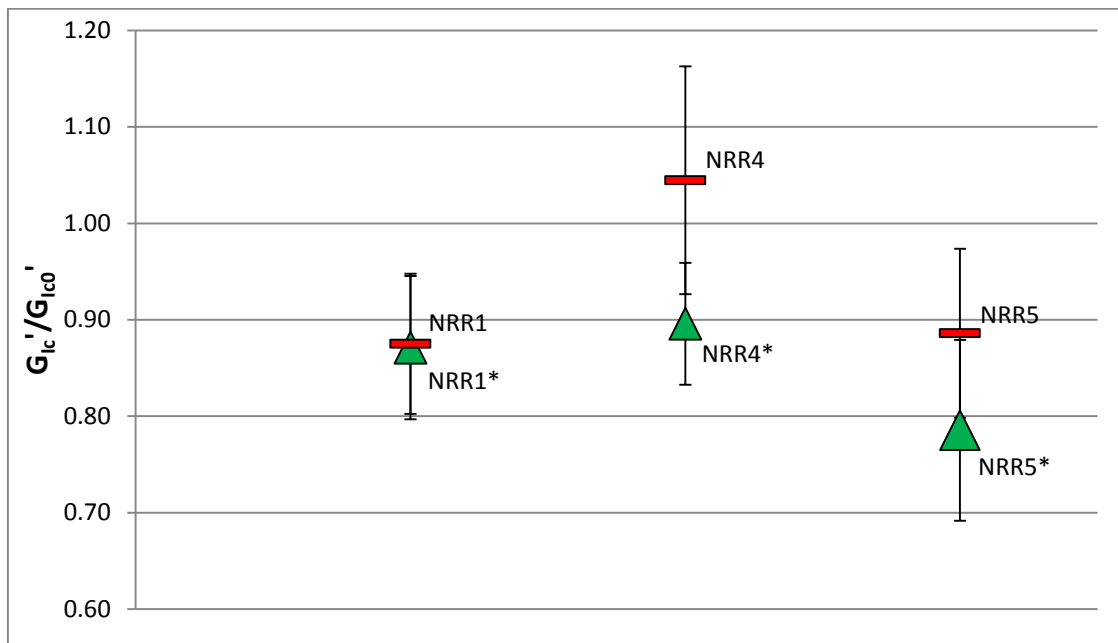


Figure 2.25. Normalized fracture toughness values from crack initiation at $a = 30$ mm for (i) complete top ply ground off case, NRR# (ii) partial top ply ground off case, NRR#*

In all three cases, the specimens consisting of repairs carried out on parent plates with the top plies ground off completely, depicted higher crack initiation toughness values at the insert tip. For repair NRR1, a significant difference was not observed.

Conclusions

DCB specimens were manufactured and tested in accordance with ASTM D5528 to screen new repair resins for wind turbine blade applications. Out of the selected resins for screening, three were initially chosen after comparing their fracture toughness values with the current repair resin. The target of this study was to find a repair resin with at least three times the fracture toughness of the current resin. However, only two times higher fracture toughness was obtained. It was also observed that parent plates repaired with the top plies partially ground off have higher propagation fracture toughness values than those with the top plies ground off completely. This phenomenon is further investigated in mixed mode I – mode II testing of repairs. The final selection of the new resin was based on fatigue testing (described in the next chapter) and on full scale testing of repairs carried out on full length blades in Europe and India. Repair resin availability on a global basis and conformation to global safety and health standards were also important criteria.

CHAPTER III

EVALUATION OF GFRP REPAIRS BY FATIGUE TESTING

Introduction

The top three new repair resin candidates NRR1, NRR4 and NRR6, selected from initial screening through mode I testing along with the base repair resin, MB-B, were tested under fatigue tensile loading to choose the final repair resin. Specimens for this part of the work were manufactured at UND but testing was carried out in Bangalore, India due to the insufficient load capacity of the fatigue testing machine at UND. Previously, in the case of mode I testing it was observed that change in grinding depth of the top ply of the parent plate affects the fracture toughness of the repair. For fatigue testing, repairs on two kinds of parent plate surfaces were evaluated. In the first case repairs were carried out without any form of grinding on the surface of the parent plate. The second case consisted of grinding the surface of the parent plate to be repaired to a whole depth of the topmost ply on either side of the plate in the region of repair.

Specimen Fabrication

Specimens for fatigue tensile testing consisted of a parent laminate with a strip of repair on either side (Figure 3.1). Eight parent plates (60 cm X 60 cm) were manufactured following same manufacturing technique (VARTM) as used for mode I testing specimens. The sequence of lay-up, curing and post curing details are listed in Table 3.1. As the lay-up was symmetric for these parent plates, no warping was observed.

Following post curing, surfaces of four of the parent plates were ground off at the regions where the repair strips were to be laid before conducting the hand lay-up with MB-B and the three chosen candidate repair resins. The repair regions were ground to one ply depth in these plates. Repairs on the other four parent plates were conducted without any grinding.

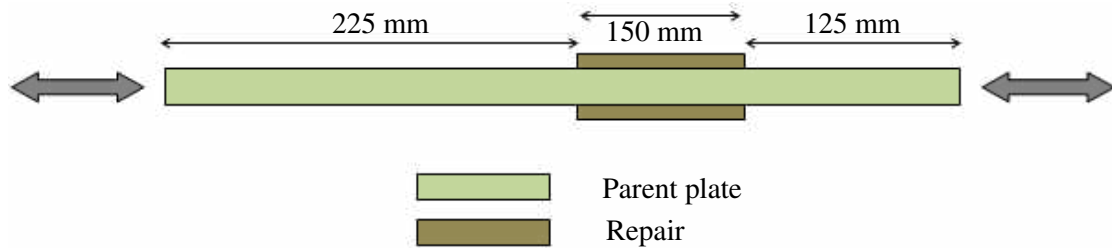


Figure 3.1. Fatigue tensile test specimen configuration (side view, not to scale)

Table 3.1. Fatigue specimen lay-up, curing and post curing details

Lay-up (top to bottom)	Part	Details
1 x Unidirectional ply (0° with CSM – CSM facing downwards)	Repair: Hand Lay-up Repair Resin	Curing: 24 hours at room temperature Post curing: 16 hrs. at 40° C
1 x Chopped strand mat (CSM)		
4 x Unidirectional ply (0° with CSM – CSM facing downwards)	Parent Laminate: VARTM Main blade resin	Curing: 24 hours at room temperature Post curing: 16 hrs. at 40° C
4 x Unidirectional ply (0° with CSM – CSM facing upwards)		
1 x Chopped strand mat (CSM)	Repair: Hand Lay-up Repair Resin	Curing: 24 hours at room temperature Post curing: 16 hrs. at 40° C
1 x Unidirectional ply (0° with CSM – CSM facing upwards)		

For each case, repair was first conducted on one side of the parent plate and left to cure at room temperature until the repair resin hardened (time depending on gel time for each repair resin) and then repair was conducted on the other side. Care was taken to procure a complete wet-out of the CSM and unidirectional glass ply repair strips and also to have the two cut edges of the same, straight. The direction of the glass fibers in the repair strip

was parallel to those in the parent plate. During the lay-up process, it was noticed that repair resin NRR1 wet-out the best and the NRR6 resin made the repair strip slip on the parent plate. There was formation of bubbles in the case of both these resins when the initiators were mixed in them respectively but the foam subsided in about 4-5 minutes. Hand lay-up was carried out after no foam was visible. The repairs were left to cure at room temperature for 24 hours and then were post cured for 16 hours at 40° C. The post cured sample plates were then cut perpendicular to the repair strip into 25 cm wide specimens (Figure 3.2).



Figure 3.2. Actual fatigue test specimen.

Fatigue Calculations and Testing

Tension – tension fatigue tests were carried out in accordance with the standard BS ISO 13003:2003 (Fibre-reinforced plastics -- Determination of fatigue properties under cyclic loading conditions.) [83]. Nine to eleven specimens were tested for each resin candidate on two servo-hydraulic fatigue machines each with a capacity to test up to a maximum load of 100 kN. Before testing, the average thickness and width of the gage area of each specimen were recorded. Lines were marked at 50 mm distance from each of the four repair ply drops A, B, C and D as shown in Figure 3.3. A specimen was considered to have failed when an interface crack originating at any of the four ply drops reached the 50 mm mark. It was assumed from observation of crack propagation in mode I testing that the crack would propagate at the repair – parent plate interface. Care was taken while mounting the specimens between the wedge grips that they were free from any bending

or misalignment. Strains in the gage area, on both faces of the specimens, were recorded with help of two extensometers (Figure 3.3). The bending ratio was calculated as the ratio of the difference to the sum $\{(\epsilon_1 - \epsilon_2) / (\epsilon_1 + \epsilon_2)\}$ of strains recorded on the opposite faces of the specimen. Bending was considered to be acceptable if the bending ratio $\{(\epsilon_1 - \epsilon_2) / (\epsilon_1 + \epsilon_2)\}$ was less than 0.1 when measured at 0.25% of the strain.

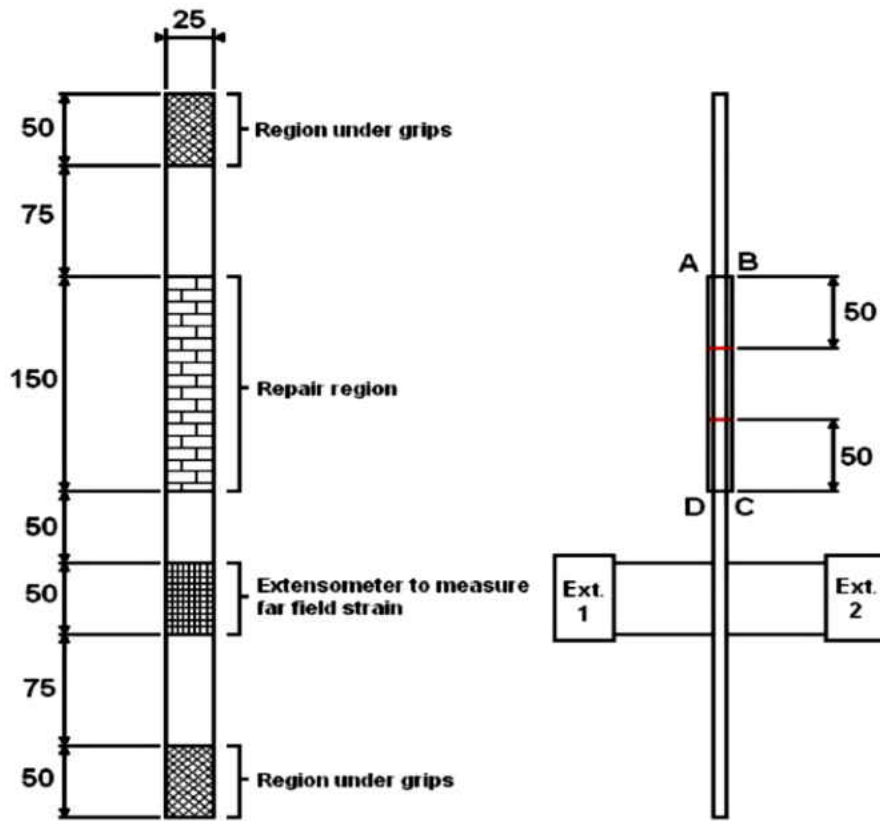


Figure 3.3. Experimental set-up of tension-tension fatigue testing (dimensions in mm)

Each specimen was first loaded in tension at the rate of 2 mm/min (stroke control) until the strain reached 0.25% and then the test was stopped. Elastic modulus was measured from the values recorded between 0.05% and 0.25% strain as

$$E = \frac{\sigma_{0.25} - \sigma_{0.05}}{0.0025 - 0.0005} \quad (3.1)$$

where $\sigma_{0.25}$ and $\sigma_{0.05}$ are the stresses at 0.25% strain and 0.05% strain respectively. For fatigue testing the specimens were loaded at a rate of 5 Hz with $R = 0.1$, where R is defined as the ratio of minimum fatigue strain to maximum fatigue strain.

Results and Discussion

In the first round of testing, specimens repaired with MB-B repair resin and with and without grinding were tested. The resulting Strain-Life (ϵ -N) and Stress-life (S-N) curves are presented in Figure 3.4 and Figure 3.5 respectively.

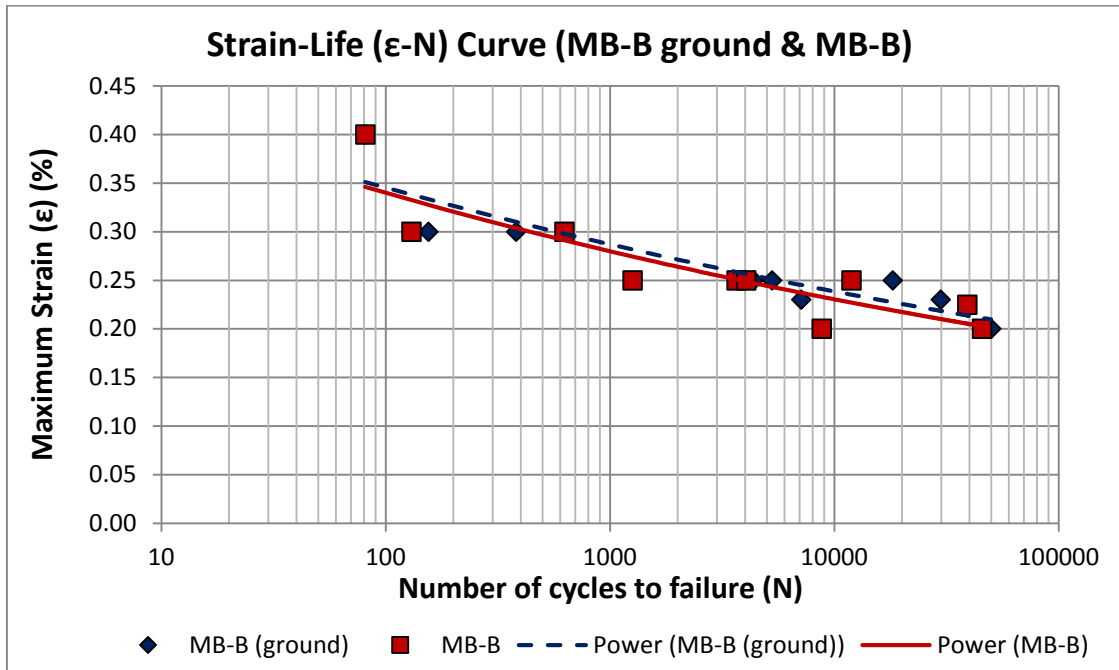


Figure 3.4. Strain-Life plot for ground (MB-B ground) and unground (MB-B) specimens

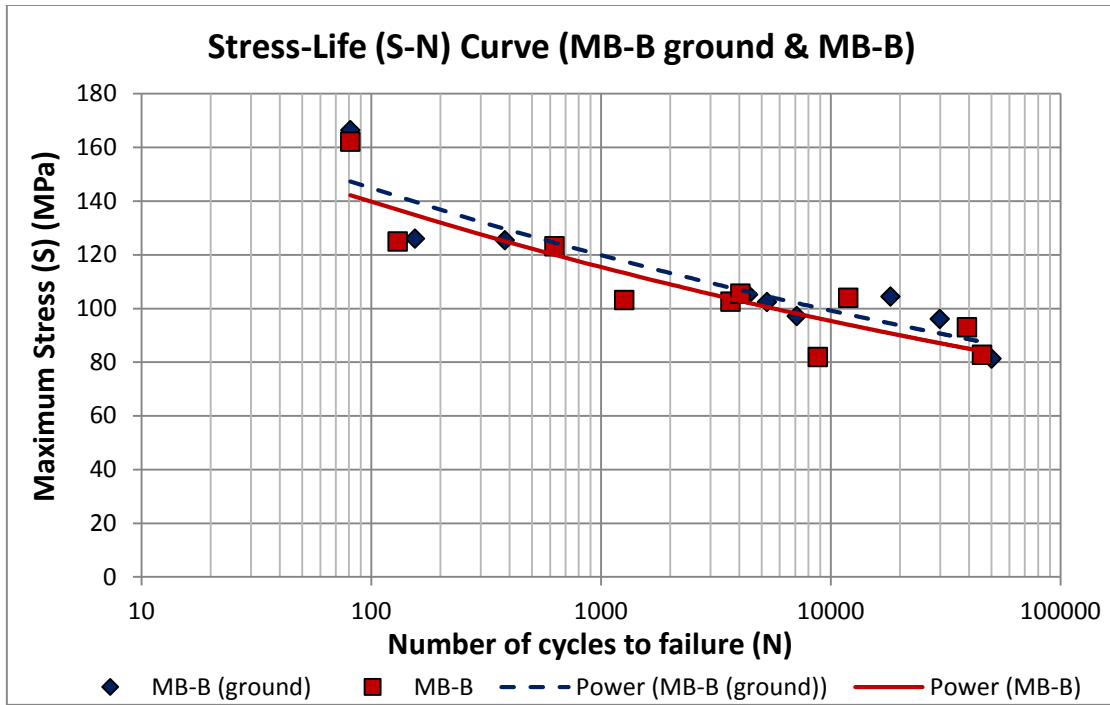


Figure 3.5. Stress-Life plot for ground (MB-B ground) and unground (MB-B) specimens

Though MB-B ground specimens do perform a little better under fatigue loads, these plots show that there is little difference in the fatigue properties of ground and unground specimens repaired by the same resin. When the region of repair on a parent plate is ground down to remove one complete ply as in the case of MB-B ground specimens, the layer of resin between the top and the second glass plies is exposed. The repair ply is then hand laminated on this freshly exposed resin layer. In the case where the top ply is not ground the repair ply is hand laminated on the resin layer present on the top surface of the parent plate. This similarity in the composition of the repair surfaces accounts for the similar fatigue characteristics in these two repair cases. Since, the ground and unground specimens did not behave very differently under fatigue, fatigue results of specimens repaired without grinding were only considered in order to avoid the effects of variation in grinding depths as those observed on fracture toughness values in mode I testing.

Strain-Life (ϵ -N) and Stress-life (S-N) curves for the repair resin candidates NRR1, NRR4 and NRR6 and their comparison with base repair resin MB-B are presented in Figure 3.6 and Figure 3.7 respectively. These depict that all three new repair resins shortlisted from mode I testing performed better than the base repair resin MB-B when loaded in tension-tension fatigue. The peak stress in NRR1 repairs at a life of about 50,000 cycles was 147 MPa which was less than the peak stresses for NRR4 (167 MPa) and NRR6 (166 MPa) at a similar life.

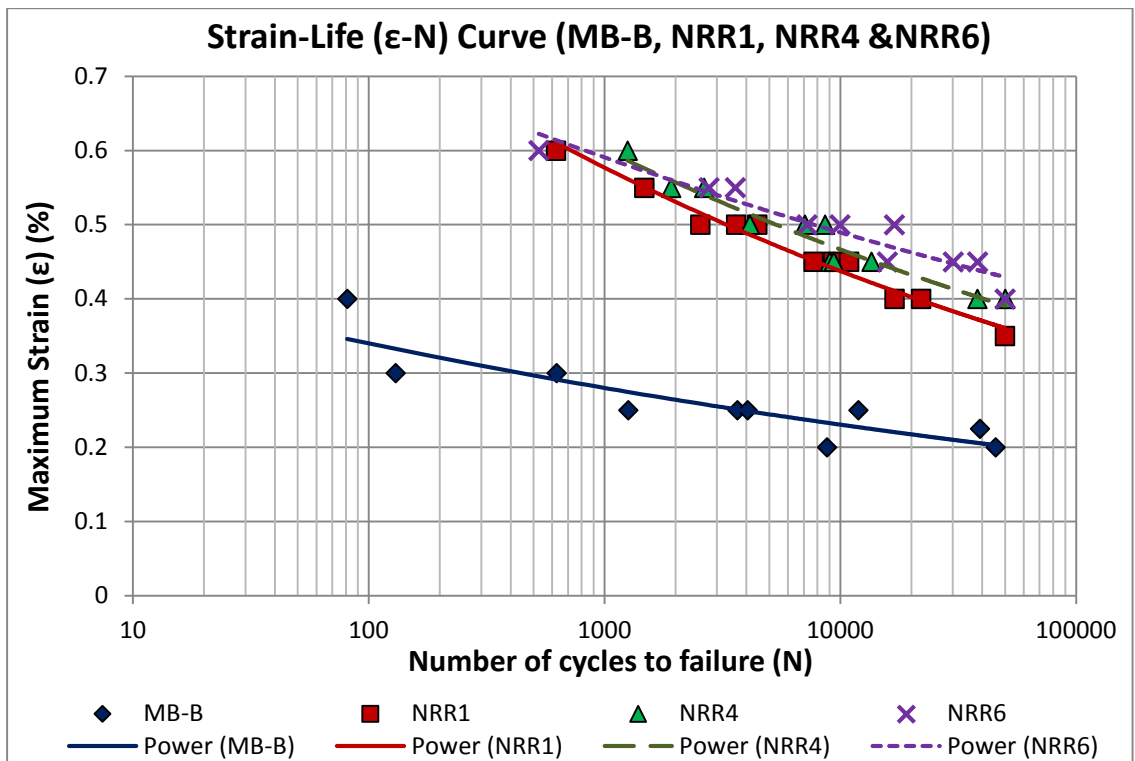


Figure 3.6. Strain –Life plot for unground specimens repaired with MB-B, NRR1, NRR4 and NRR6 repair resins

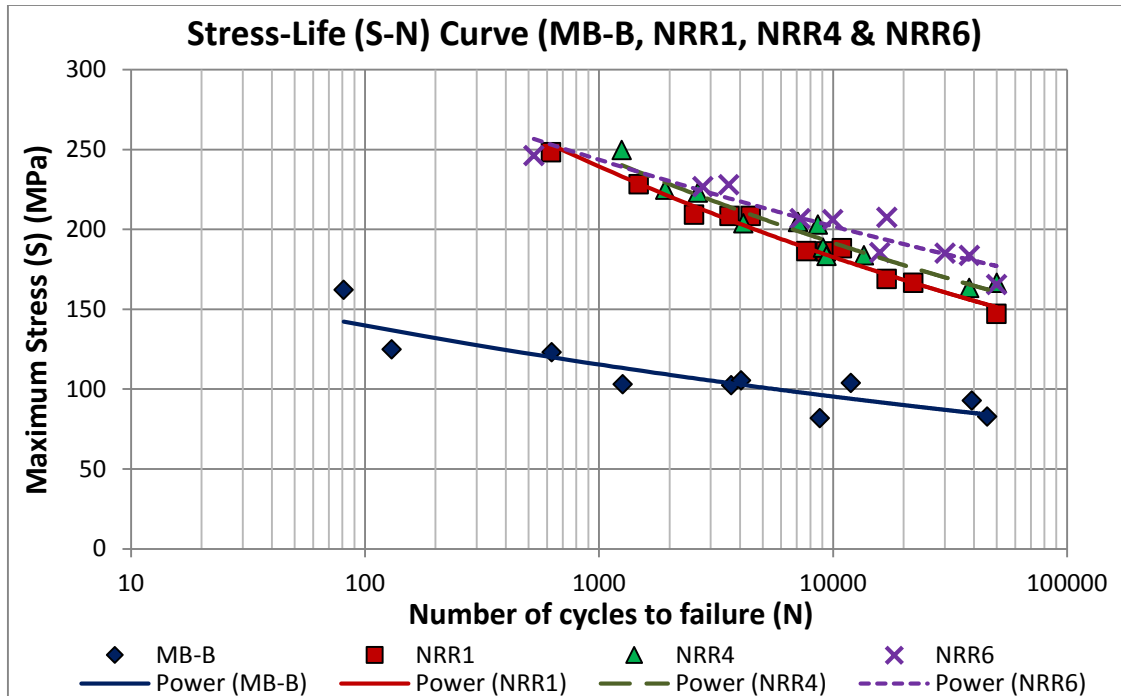


Figure 3.7. Stress –Life plot for unground specimens repaired with MB-B, NRR1, NRR4 and NRR6 repair resins

From Mode I and tension-tension fatigue testing results NRR4 was selected as the final new repair resin as it is already being produced in accordance with global standards and safety regulations. NRR6 is being manufactured only in the US and does not possess European certifications.

CHAPTER IV

STUDY OF REPAIR PARAMETERS BY MIXED MODE I – MODE II TESTING

Specimen Manufacturing and Preparation

Initial testing specimens

Specimens for preliminary mixed mode I – mode II testing were similar in lay-up to those for mode I testing but with different dimensions. Parent plates were made using VARTM and were ground down to a depth of one ply and repairs were conducted on the exposed surface obtained. Repair resins MB-B, NRR4 and NRR6 were used to conduct repairs on the parent plates. A description of the lay-up and the materials used is given in Table 4.1.

Table 4.1. Initial mixed mode I – mode II specimen lay-up, materials used and curing details

Lay-up	Part	Details
2 x Biaxial plies ($\pm 45^\circ$)	Repaired Laminate: Hand Lay-up MB-B, NRR4 & NRR6 (Upper adherend)	Curing: 24 hours at room temperature Post curing: 16 hrs. at 40°C
8 x Unidirectional plies (0° , E-glass with CSM)		
1 x Chopped strand mat		
Insert (Crack Initiator)	Polymer film	Thickness $\leq 13 \mu\text{m}$
8 x Unidirectional plies (0° , E-glass with CSM)	Parent Laminate: VARTM MB-A (Lower adherend)	Curing: 24 hours at room temperature Post curing: 24 hrs. at 60°C 3 hrs. at 95°C
2 x Biaxial plies ($\pm 45^\circ$)		

Subsequent testing specimens

For initial testing, specimens were made with the same materials and average thickness of $h \sim 9$ mm (Figure 4.1) as the DCB specimens for mode I testing. Mixed-mode ratios (G_{II}/G_c) of 0.2, 0.5 and 0.8 were used. It was found that the adhesive bond of the piano hinges with the specimen was not able to bear the loads (1.5 ± 0.15 kN) incurred at 0.5 and 0.8 values of G_{II}/G_c . The range of the thickness h of each adherend (Figure 4.1) was recalculated for the required maximum load < 1.5 kN, keeping in consideration that the displacements were not so large as to cause geometric nonlinear errors [61]. The final specimen thickness obtained from the results of the initial mixed mode I – mode II testing and calculations from ASTM D 6671/D 6671M – 06 using estimated critical load and load point deflection values was $h \sim 5$ mm, a reduction of approximately 4 mm from the thickness of each adherend of a mode I testing specimen.

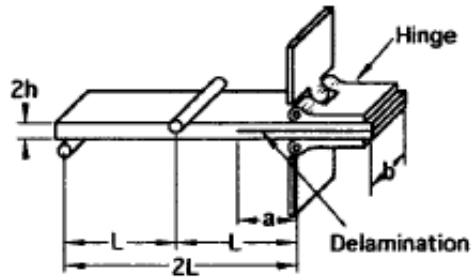


Figure 4.1. Specimen details for mixed mode I – mode II test [61]

The specimens for subsequent testing were manufactured using a different quality of glass fibers compared to that (E-glass) used to make specimens for mode I and fatigue testing. This glass, termed H-glass for the rest of this report, is currently being used by LM Windpower to manufacture wind turbine blades of length more than 50 meters. H-

glass possesses better mechanical properties than the E-glass previously used. It does not have a chopped strand mat (CSM) as a backing material and is composed mainly of unidirectional glass fibers. The parent plates initially comprised of six plies with average thickness of 5.3 ± 0.1 mm. They were manufactured using VARTM and a new main blade resin MB-A' that is now being used by LM Windpower to manufacture wind turbine blades. The main blade resin MB-A' is similar in chemical composition to MB-A but is manufactured by a different company. The parent plates were cured at room temperature for 24 hours and then post-cured in an oven at 60° C for 24 hours and then at 95° C for 3 hours to ensure that the plates had the same degree of cure.

In order to investigate the effect of variation in grinding on the mixed-mode fracture toughness of the repairs, complete top plies in one set of four parent plates and partial top plies in the other set of four parent plates were ground off. During specimen preparation for the mode I testing it was noticed that the gel time for NRR4 was around 120 minutes (Table 2.3). This amount of gel time is not conducive for hand repairs on vertical surfaces. In order to reduce the gel time, changes were made to the chemical composition of NRR4 to decrease the gel time to 35 minutes. Details of changes to chemical composition are not known due to proprietary reasons. Repairs for the later mixed mode I – mode II testing were carried out by using MB-B and the modified NRR4 repair resin (NRR4'). A polymer insert (thickness < 13 μ m) similar to the one used in mode I specimens was used to create a pre-crack of 25 mm at the resin inlet during repair. The delaminated section of the specimen was 75 mm in length and the hinges were applied so as to have the load line at a distance of 25 mm from the pre-crack tip. Details of the configuration and materials used to make the specimens are given in Table 4.2. Figure

4.2 depicts, (a) the methods of manufacturing of the parent plates, (b & c) surface preparation for repairs and (d & e) repairs being conducted. The repairs were carried out in a similar fashion to that in the case of mode I testing and were allowed to cure at room temperature for 24 hours. Then, post-curing was carried out for 16 hours in the oven at 40° C. After the parent plates had been repaired and cured, they were found to be slightly warped in a direction perpendicular to the unidirectional fibers. This was most probably due to the difference in the composition of the parent plate and repair resins and the shrinkage of the repair resin while in contact with the pre-cured parent plate resin. Again, as in the mode I testing, it was assumed that this warp would not have a significant effect on the test results since the specimens were to be cut in a direction along the unidirectional glass fibers.

Table 4.2. Subsequent mixed mode I – mode II specimen lay-up, materials used and curing details

Lay-up	Part	Details
5 x Unidirectional plies (0°, H-glass)	Repaired Laminate: Hand Lay-up MB-B & NRR4' (Upper adherend)	Curing: 24 hours at room temperature
1 x Chopped strand mat		Post curing: 16 hrs. at 40° C
Insert (Crack Initiator)	Polymer film	Thickness ≤ 13 μm
5 x Unidirectional plies (0°, H-glass)	Parent Laminate: VARTM MB-A' (Lower adherend)	Curing: 24 hours at room temperature Post curing: 24 hrs. at 60° C 3 hrs. at 95° C



4.2 (a) VARTM



4.2 (b) Grinding



4.2 (c) Repair surface preparation



4.2 (d) Resin application



4.2 (e) Removal of voids

Figure 4.2. Mixed-mode specimen manufacturing

The repaired plates were sectioned into 25 mm wide and 250 mm long specimens with premium grade carbide toothed saw. Plexus MA300 (methacrylate adhesive) was used to bond piano hinges to the specimens. The surface areas of the specimens where the hinges were to be glued were sanded lightly and then wiped clean with acetone in order to achieve a strong bond. The hinges were aligned parallel with the specimen and held in position with the help of clamps while the adhesive cured. The edges of the specimens were coated with a water-based white typewriter fluid and thin lines were marked every 1 mm for a distance of 30 mm from the end point of the pre-crack. Along the load line a speckled pattern was created on the specimen. The mm markings were done in order to make it easier to monitor crack propagation. The speckled pattern was created on each specimen in order for Vic-2D Correlation Software to be able to correlate the pictures obtained to calculate the stroke displacement that occurred during each test.

Testing and Calculations

All mixed mode I – mode II testing was carried out in accordance with the Standard Test Method for Mixed Mode I – Mode II Interlaminar Fracture Toughness of Unidirectional Fiber Reinforced Polymer Matrix Composites (ASTM D 6671/D 6671M – 06) [61]. The

mixed mode I – mode II bending test apparatus shown in Figure 4.3 is used to pull apart the two adherends of the DCB specimens in order to calculate the mixed-mode delamination fracture toughness values at different ratios of mode I to mode II loading. The specimen is supported at the base by the hinge attachment at the delaminated section and by a roller at the other end. The roller attached to the lever arm bears on the top surface of the specimen at a distance midway between the base roller and the hinges. Loads are applied to the delaminated part of the specimens (that contains the pre-crack) by pulling at the hinges and also through rollers that bear against the specimen in the non-delaminated section of the specimen. This setup results in application of mode I load at the hinges and mode II load at the fulcrum formed by the roller attached to the lever arm.

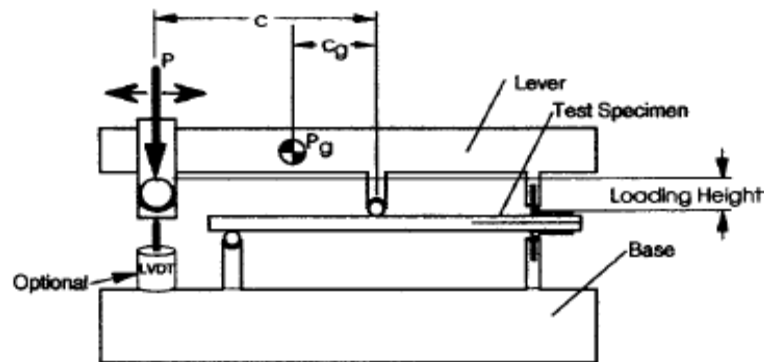


Figure 4.3. Test fixture and parameters of mixed-mode test [61]

Three specimens were tested at each mixed mode ratio for all cases. Specimens were mounted on the mixed mode I – mode II (ASTM D 6671/D 6671M – 06) test fixture and testing was carried out on the Shimadzu AG-IS Universal Testing Machine under displacement control at a crosshead rate of 0.5 mm/min. Loads were recorded using TRAPEZIUM 2 control software linked to the universal testing machine and images of the loaded samples were captured with a Retiga 1300 camera using the Vic-Snap

software. These images were analyzed for stroke displacements using Vic-2D Digital Image Correlation Software. A picture of a specimen being tested in the (ASTM D 6671/D 6671M – 06) fixture is given in Figure 4.4.

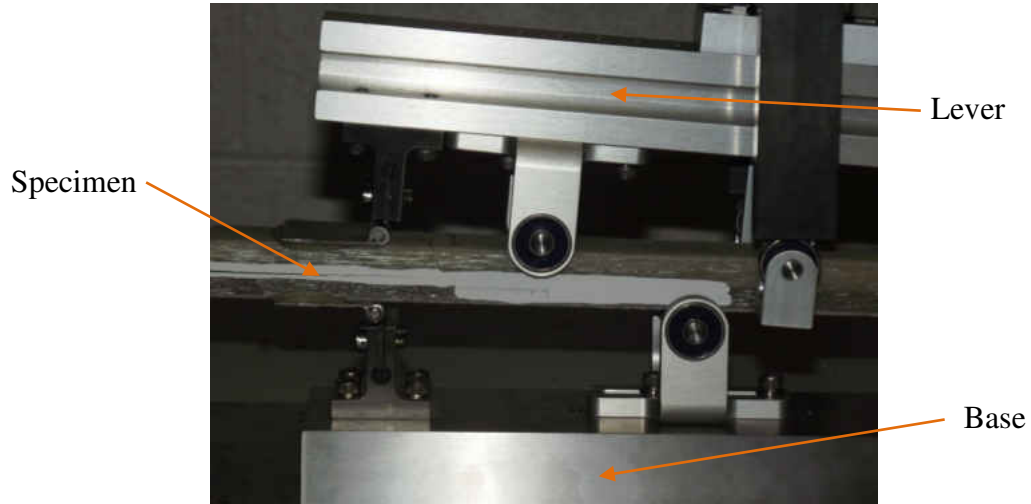


Figure 4.4. Mixed mode I – mode II test snapshot

Before testing, the length, c (Figure 4.3), of the lever of the mixed mode I – mode II test fixture was calculated and set to produce the desired mode mixture ratio G_{II}/G in accordance with Equation 4.1 as given in (ASTM D 6671/D 6671M – 06):

$$c = \frac{12\beta^2 + 3\alpha + 8\beta\sqrt{3\alpha}}{36\beta^2 - 3\alpha} L \quad (4.1)$$

where

$$\alpha = \frac{1 - \frac{G_{II}}{G}}{\frac{G_{II}}{G}} \quad (4.2)$$

and

$$\beta = \frac{a + \chi h}{a + 0.42\chi h} \quad (4.3)$$

where a is the crack length. The crack length correction parameter χ is given by Equation 4.4:

$$\chi \equiv \sqrt{\frac{E_{11}}{11G_{13}} \left\{ 3 - 2 \left(\frac{\Gamma}{1+\Gamma} \right)^2 \right\}} \quad (4.4)$$

where Γ , the transverse modulus correction parameter, is calculated as

$$\Gamma = 1.18 \frac{\sqrt{E_{11}E_{22}}}{G_{13}} \quad (4.5)$$

and E_{11} = longitudinal modulus of elasticity measured in tension (MPa), E_{22} = transverse modulus of elasticity (MPa) and G_{13} = shear modulus out of plane (MPa). The half-span length, L , (Figure 4.1) of the mixed mode I – mode II testing fixture was kept 50 mm for all mode mixity ratios. Thus, crack propagation was observed to a distance of 25 mm from the pre-crack tip i.e. to a distance of 50 mm from the load line. After testing had been conducted the flexural modulus was calculated as:

$$E_{1f} = \frac{8(a_0 + \chi h)^3 (3c - L)^2 + [6(a_0 + 0.42\chi h)^3 + 4L^3](c + L)^2}{16L^2 b h^3 \left(\frac{1}{m} - C_{sys} \right)} \quad (4.6)$$

where a_0 = the initial delamination length (mm), m = slope of load displacement curve (N/mm), b = width of specimen (mm), C_{sys} = system compliance (mm/N), and L = half span length of the test apparatus (mm) (Figure 4.1). The fracture toughness and mode mixture were calculated using the equations given below:

$$G_I = \frac{12P^2(3c-L)^2}{16b^2h^3L^2E_{1f}} (a + \chi h)^2 \quad (4.7)$$

$$G_{II} = \frac{9P^2(c+L)^2}{16b^2h^3L^2E_{1f}} (a + 0.42\chi h)^2 \quad (4.8)$$

$$G = G_I + G_{II} \quad (4.9)$$

$$\frac{G_{II}}{G} = \frac{G_{II}}{G_I + G_{II}} \quad (4.10)$$

where G_I = mode I component of strain energy release rate (kJ/m²), G_{II} = mode II component of strain energy release rate (kJ/m²) and G = total mixed-mode strain energy release rate (kJ/m²). In the case of calculations related to delamination growth, the strain

energy rate equals the fracture toughness when a critical load, P_c , is used instead of P , the applied load measured in N.

Results and Discussion

Initial Testing

From the initial mixed-mode testing for mixed mode load ratio $G_{II}/G = 0.2$, fracture toughness values of crack propagation for the repair resins MB-B and NRR4 were plotted against crack length (Figures 4.5 (a) – (b)). Preliminary results show that fracture toughness values obtained with delamination growth in accordance with ASTM D 6671/D 6671M – 06 are higher for NRR4 as compared to MB-B. This corroborates with the results obtained from mode I and fatigue testing for these two repair resins.

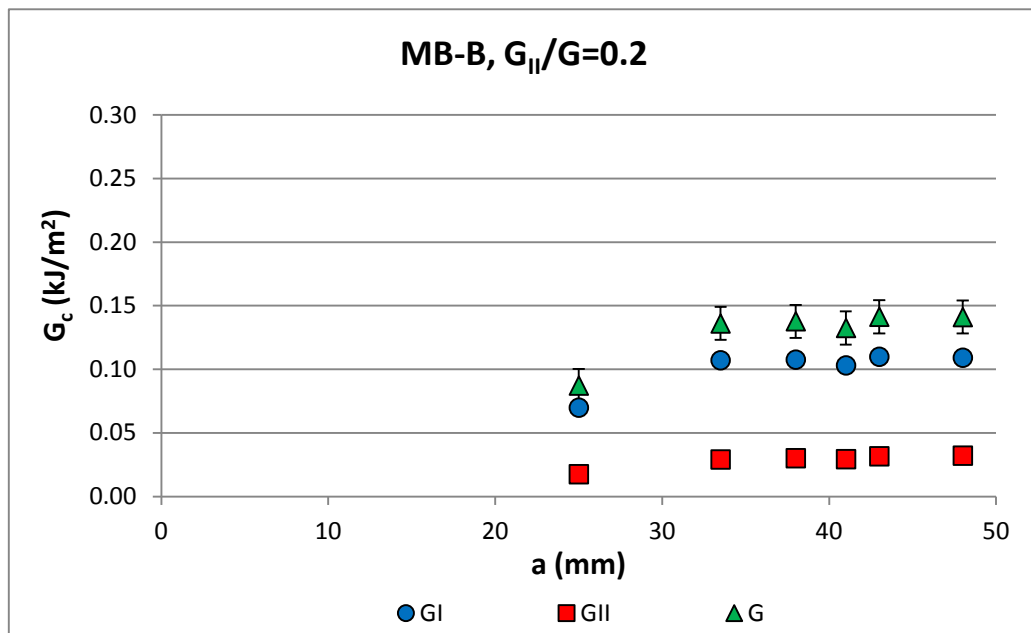


Figure 4.5. (a) Preliminary mixed mode I – mode II testing results for current blade repair resin MB-B

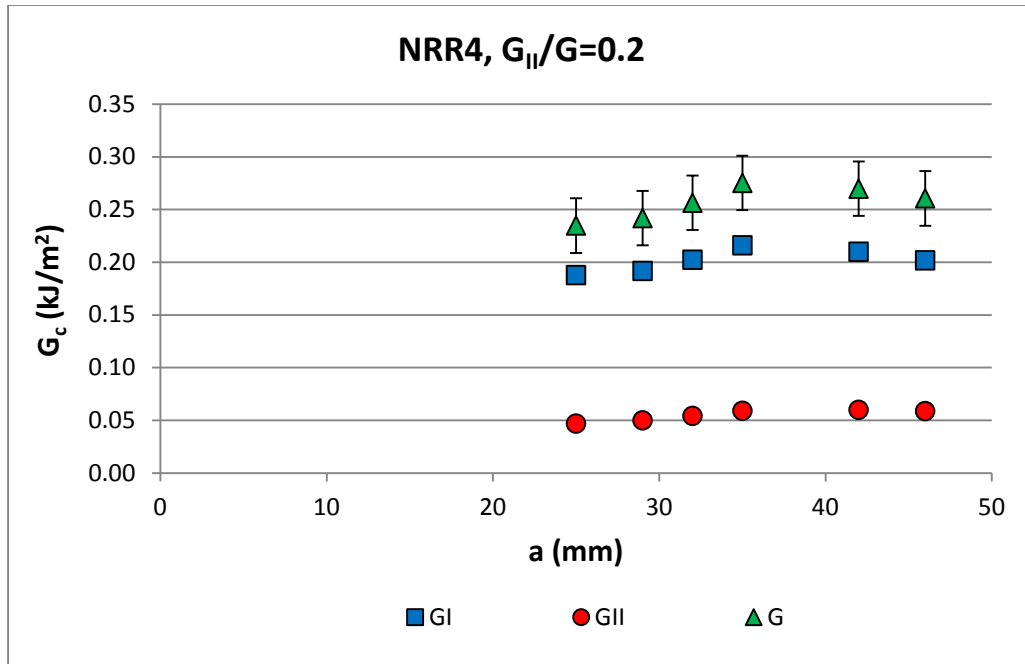


Figure 4.5. (b) Preliminary mixed mode I – mode II testing results for new repair resin candidate NRR4

The fracture toughness values corresponding to their respective crack lengths for the two resins are tabulated in Table 4.3 and Table 4.4. At crack initiation, NRR4 has a much higher fracture toughness value (more than double) than that of MB-B. Other than the difference in the chemical compositions of the two resins (higher styrene content in NRR4) that result in a stronger bond in the case of NRR4, this higher value may also partially be attributed to the presence of fiber bridging that is evident in NRR4 starting right from the end of the pre crack (Figure 4.6). Though some fiber bridging begins later, at about 10 mm, from the crack tip in the case of MB-B, (Figure 4.6) it is not able to increase the subsequent fracture toughness values to an extent so as to be comparable to those of NRR4.

Table 4.3. Fracture toughness ($G_{II}/G = 0.2$) values for MB-B

a (mm)	G_I (kJ/m²)	G_{II} (kJ/m²)	G_c (kJ/m²)
25 ± 0.5	0.070 ± 0.007	0.017 ± 0.003	0.087 ± 0.010
33.5 ± 0.5	0.107	0.029	0.136
38 ± 0.5	0.108	0.030	0.138
41 ± 0.5	0.103	0.029	0.132
43 ± 0.5	0.110	0.032	0.141
48 ± 0.5	0.109	0.032	0.141

Table 4.4. Fracture toughness ($G_{II}/G = 0.2$) values for NRR4

a (mm)	G_I (kJ/m²)	G_{II} (kJ/m²)	G_c (kJ/m²)
25 ± 0.5	0.188 ± 0.002	0.047 ± 0.003	0.235 ± 0.005
29 ± 0.5	0.192	0.050	0.242
32 ± 0.5	0.202	0.054	0.256
35 ± 0.5	0.216	0.059	0.275
42 ± 0.5	0.210	0.060	0.270
46 ± 0.5	0.202	0.059	0.261

In the case of mixed mode I – mode II testing of specimens repaired with repair resin NRR6, the crack propagation was very fast and the camera was not able to capture the crack length values between the 25 mm and 50 mm marks. Thus it was not possible to record the propagation fracture toughness values for this resin. The reason for the fast crack growth can be the lack of fiber bridging as can be seen in Figure 4.6. NRR6 showed better crack initiation fracture toughness values than the repair resin MB-B (Figure 4.7) but they were less than those for NRR4.

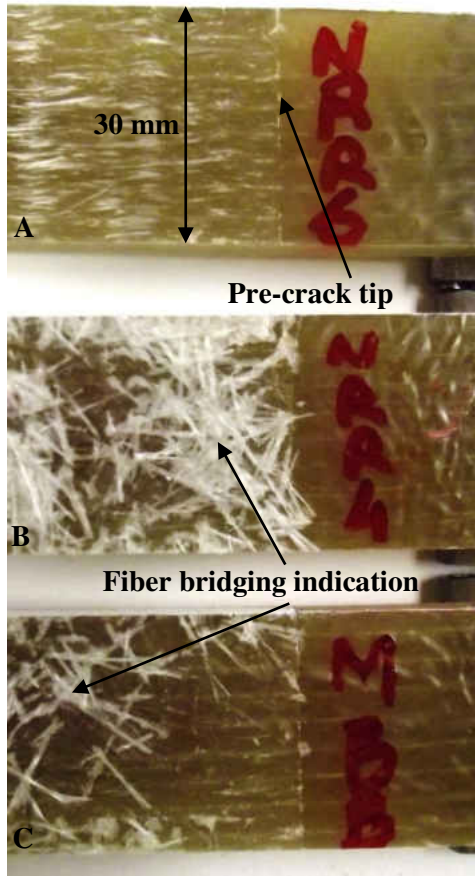


Figure 4.6. Fiber bridging in NRR6 (specimen A), NRR4 (specimen B) and MB-B (specimen C) in mixed mode I – mode II ($G_{II}/G_c = 0.2$) test

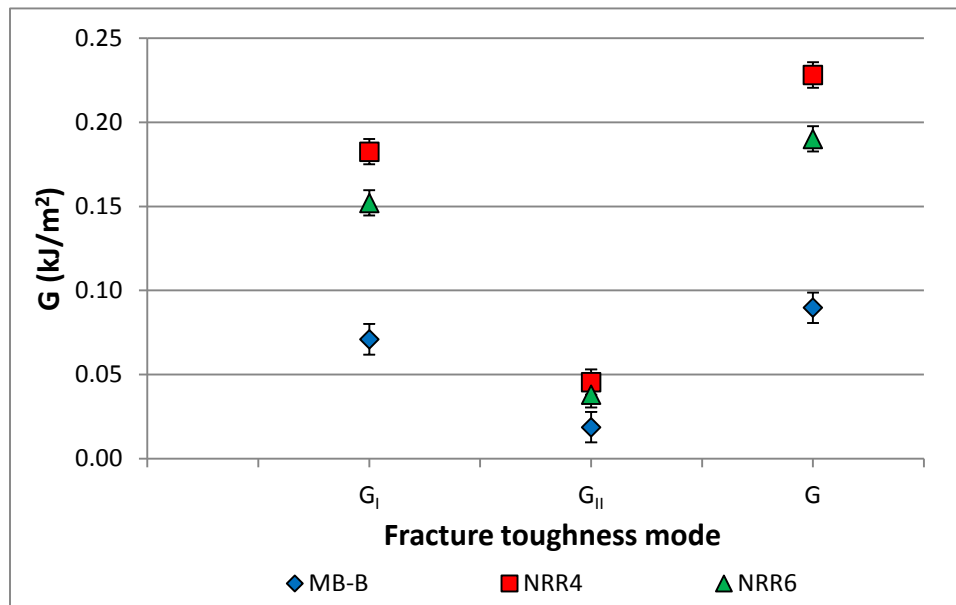


Figure 4.7. Fracture toughness values at crack initiation for MB-B, NRR4 and NRR6

Subsequent Testing

Specimens consisting of parent plates manufactured with MB-A' and H-glass and repaired with MB-B and NRR4' repair resins were tested after the initial mixed mode I – mode II testing. The length of the lever arm, c , of the mixed mode I – mode II testing apparatus was varied for each of the mode mixtures ($G_{II}/G = 0.2, 0.5$ and 0.8) before testing. Two levels of grinding of the top ply of the parent plate were evaluated. In mode I testing it was seen that difference in grinding depth of the top surface of the parent plate while preparing it for repairs does affect the fracture toughness values of the repairs. For this testing one set of plates was repaired with the top unidirectional glass-fiber ply completely ground off, thus exposing a surface comprising mainly of cured resin as shown in Figure 4.8 (a). The top unidirectional glass-fiber ply of the other set was partially ground off to expose a surface comprising of a mixture of glass fibers and cured resin (Figure 4.8 (b)).

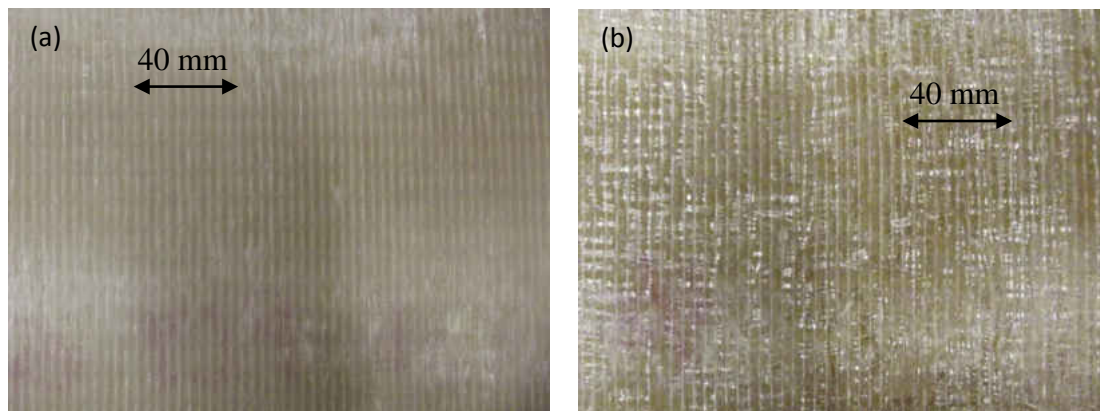


Figure 4.8. Parent plate with (a) complete top ply ground off (b) partial top ply ground off

Delamination fracture toughness values, calculated from the critical loads obtained from testing, were plotted as a function of mode mixtures for the different resins and grinding levels. It was not possible to plot the delamination propagation fracture toughness values

as the crack growth was very fast in mixed-mode testing. A typical fracture toughness contour is shown in Figure 4.9 for the repair carried out using repair resin MB-B after grinding off the top ply of the parent plate completely. The delamination fracture toughness values increase with an increase in the percentage of mode II loading from 20% to 80% as expected.

The scatter in the toughness values does not bear a linear relation with the increase in mode II percentage. As shown in the plot, the mixed mode fracture toughness values obtained at different mode II ratios can be generally fitted by an exponential curve. Similar trend was found by Benzeggagh and Kenane [66] and further corroborated by other researchers like Dharamawan et al [70].

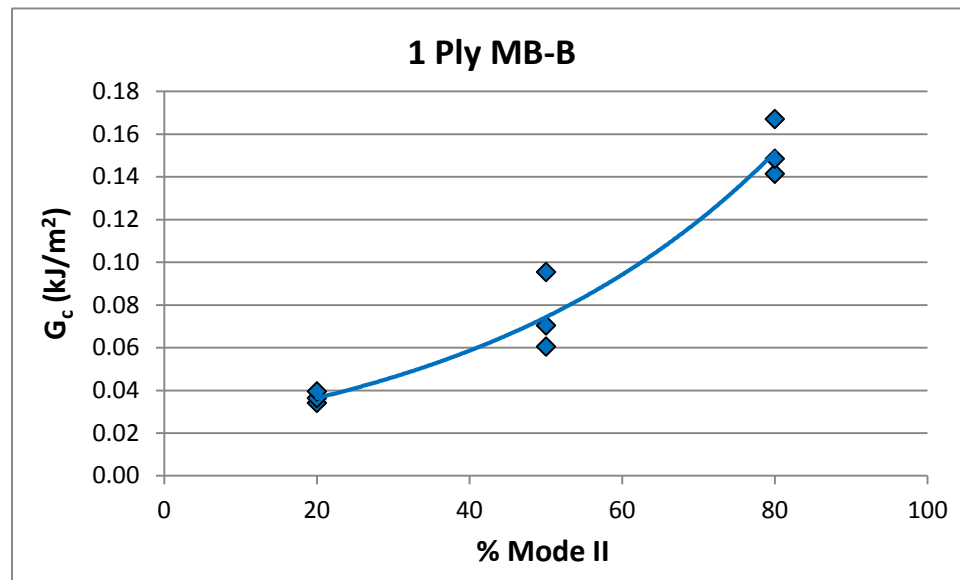


Figure 4.9. Delamination fracture toughness values for MB-B with whole top ply of parent plate ground off

Similar fracture toughness contours are shown in Figures 4.10 – 4.12 for resin MB-B with partial top ply ground off, and resin NRR4' with complete top ply ground off and resin NRR4' with partial top ply ground off, respectively.

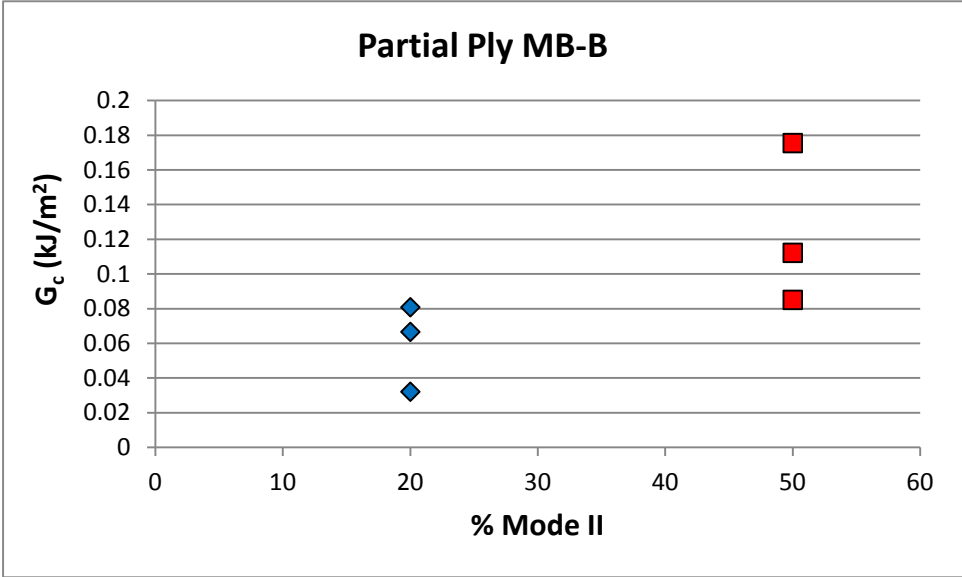


Figure 4.10. Delamination fracture toughness values for MB-B with partial top ply of the parent plate ground off

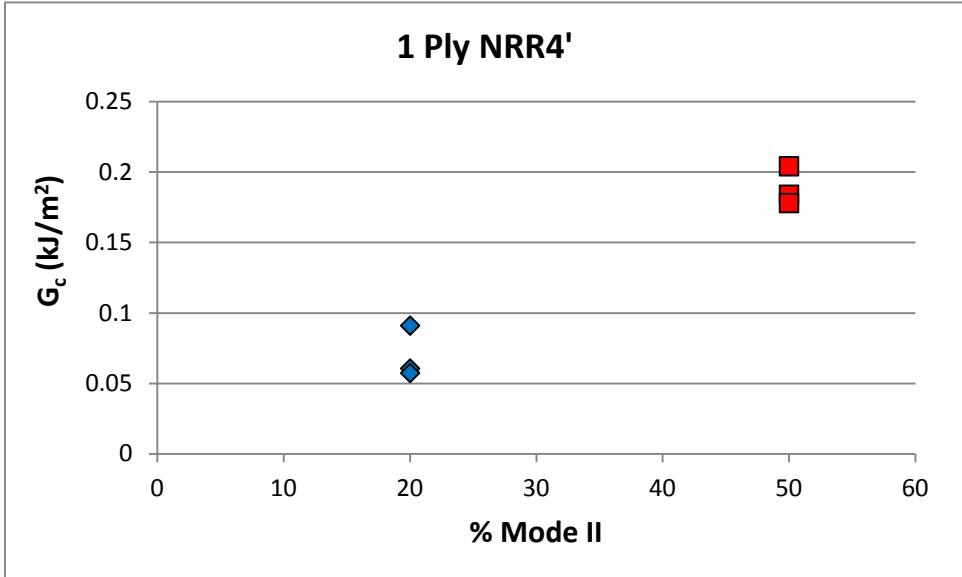


Figure 4.11. Delamination fracture toughness values for NRR4' with whole top ply of parent plate ground off

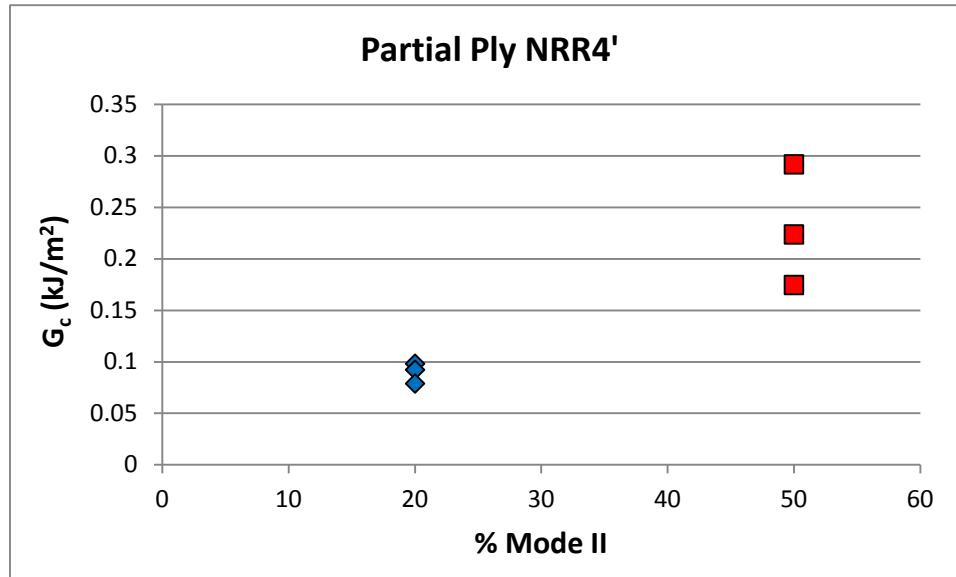


Figure 4.12. Delamination fracture toughness values for NRR4' with partial top ply of the parent plate ground off

In all of these three cases (Figures 4.10 – 4.12) the methacrylate adhesive used to bond the hinges to the composite specimens was not able to bear the high shear loads at mode mixity ratio $G_{II}/G = 0.8$ and the hinges came off the specimens before crack initiation. The values of delamination fracture toughness for the mode mixity ratio $G_{II}/G = 0.8$ for these specimens were not recorded. The loads at which the hinges came off were of the order of 1.55 ± 0.15 kN. These loads were similar to the loads experienced by the initial mixed mode I – mode II testing specimens (with each adherend thickness ~ 9 mm) when they were tested at mode mixity ratio $G_{II}/G = 0.5$. Equation 4.11 from ASTM D 6671/D 6671M – 06 that was used to estimate the thickness of the specimens so that they would be able to bear the $G_{II}/G = 0.8$ loads does not take into account the fracture toughness of the bond between the composites and the methacrylate adhesive. It takes into account only G_c^{est} which is the estimated value of the composite total mixed mode fracture toughness.

$$P^{est} = \sqrt{\frac{\frac{4}{3}G_c^{est}b^2E_{11}h^3L^2}{(3c-L)^2(a+h\chi)^2 + \frac{3}{4}(c+L)^2(a+0.42h\chi)^2}} \quad (4.11)$$

A load of 0.752 kN (Table 4.5) was taken to accommodate for the fracture toughness of the methacrylate adhesive and accordingly adherend thickness h was chosen to be 5 mm. The new adherend thickness $h \sim 5$ mm was considered corresponding to a load that was half the critical load value of 1.5kN found out for the hinges during initial testing. Even then, it was not suitable for testing at mixed mode ratio $G_{II}/G = 0.8$ for the specimens manufactured with H-glass and NRR4' repair resin and the MB-B specimens with the partial top ply ground off. A smaller thickness of each adherend approximately 2~3 mm may be required for the hinges to be able to bear the high mode II loads.

Table 4.5. Estimated load values calculated using Equation 4.11 for different values of h

G_{II}/G	P^{est} (N)							
0.2	39.7	110.6	199.8	302.7	416.4	538.8	668.57	804.5
0.5	61.0	169.9	307.0	465.1	639.7	827.8	1027.2	1236.1
0.8	71.8	199.7	360.9	546.7	752.0	973.2	1207.6	1453.2
h (mm)	1	2	3	4	5	6	7	8

Results from the mixed mode G_{II}/G_c ratios of 0.2 and 0.5 (Figure 4.13 and Figure 4.14) show that specimens repaired with NRR4' exhibit higher delamination fracture toughness values in mixed mode I – mode II testing as compared to those repaired with MB-B. In case of both repair resins, specimens repaired with partial top plies of the parent plates ground off have better fracture toughness values than the repairs with the complete top plies of the parent plates ground off. Similar phenomenon was observed in the case of mode I testing.

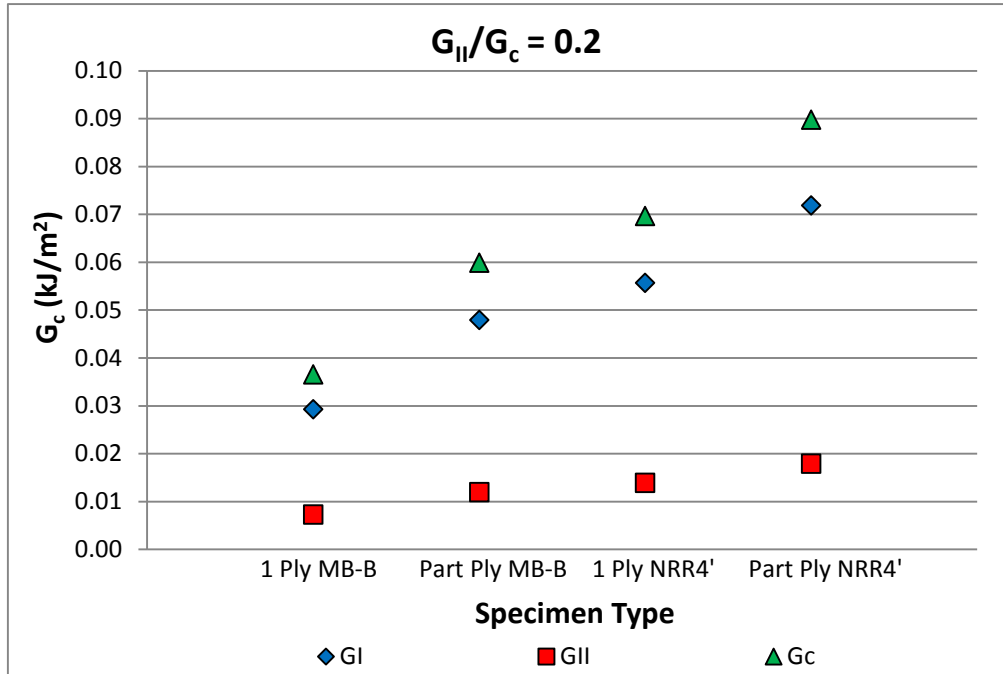


Figure 4.13. Fracture toughness values for MB-B and NRR4' at different grinding levels under mode II 20% loads (1 Ply ~ Complete top ply ground off, Part Ply ~ Partial top ply ground off)

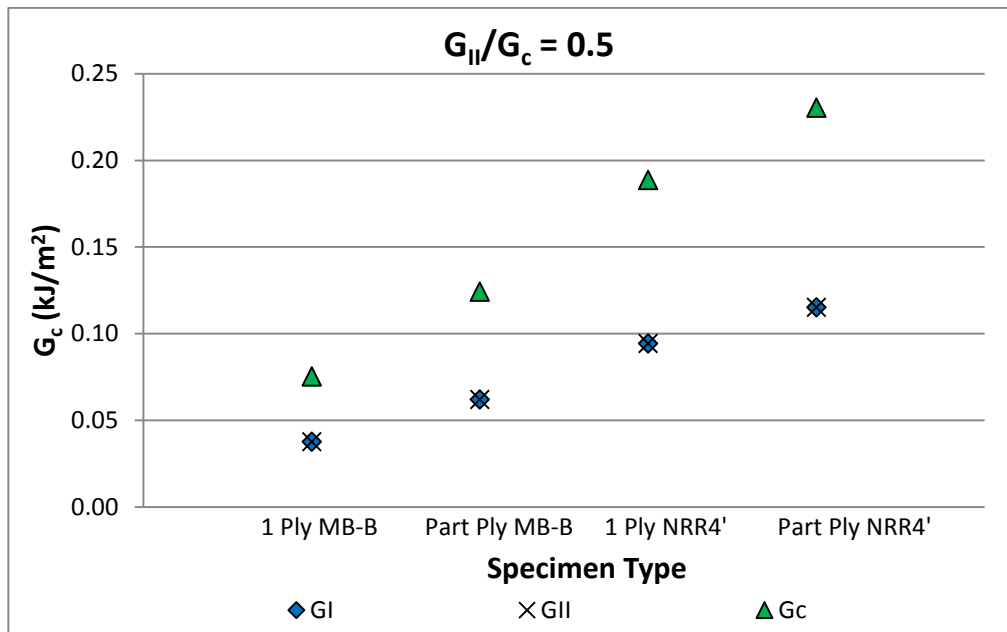


Figure 4.14. Fracture toughness values for MB-B and NRR4' at different grinding levels under mode II 50% loads (1 Ply ~ Complete top ply ground off, Part Ply ~ Partial top ply ground off)

Images of the fractured surfaces of specimens tested under various mixed mode ratios are shown in Figure 4.15. The MB-B specimens that were tested with mixed mode ratio $G_{II}/G = 0.2$, do not show significant signs of fiber bridging or effects of mode II load (Figure 4.15 (a) and (e)). In the case of MB-B specimens tested with mixed mode ratio $G_{II}/G = 0.5$, there are some signs of plastic deformation of the repair resin (depicted by white regions) under shear loads (Figure 4.15 (b)). For mode II 80% loads the MB-B specimens have more pronounced signs of fiber bridging as well as deformation of the repair resin due to shear loads.

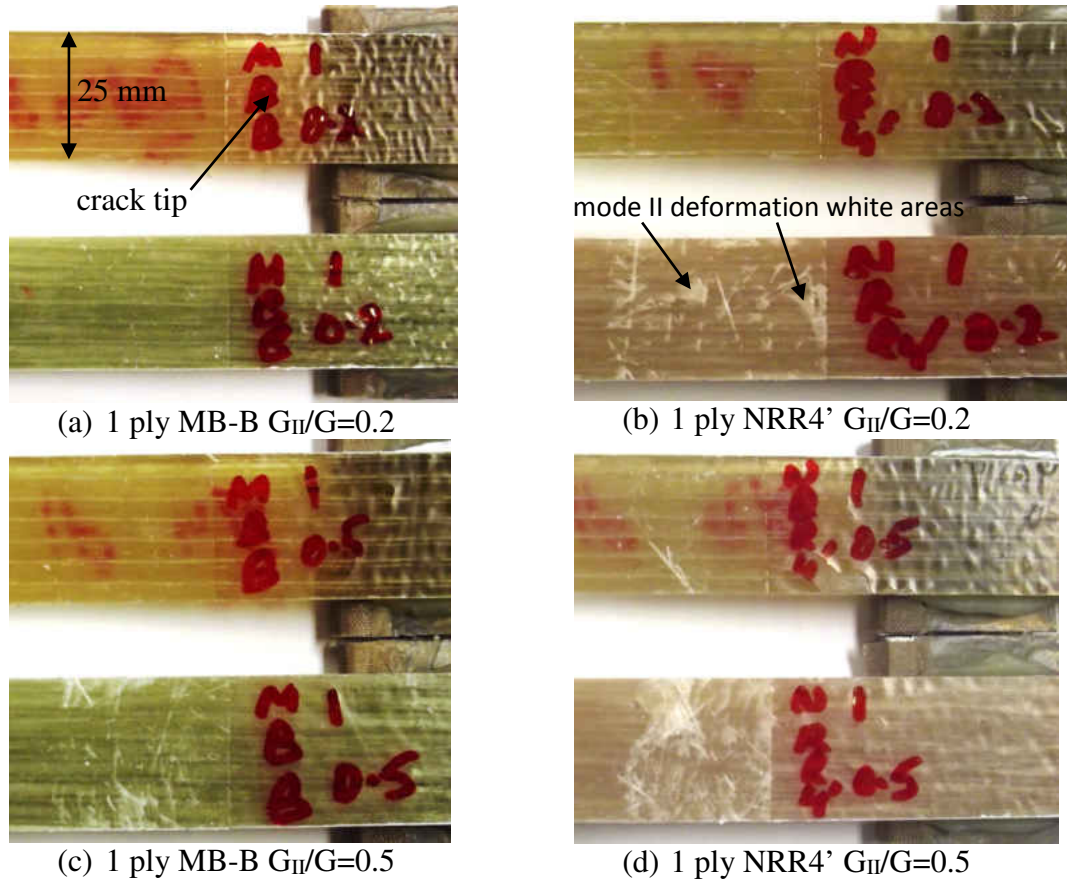
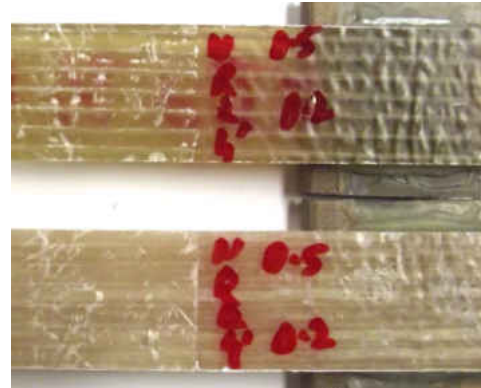


Figure 4.15. Images of surfaces fractured under different mixed mode I – mode II loads

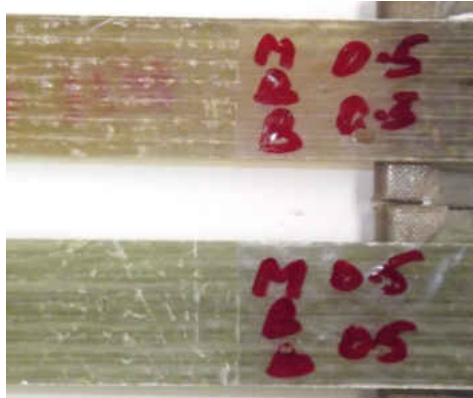
Figure 4.15 cont.



(e) Partial ply MB-B $G_{II}/G=0.2$



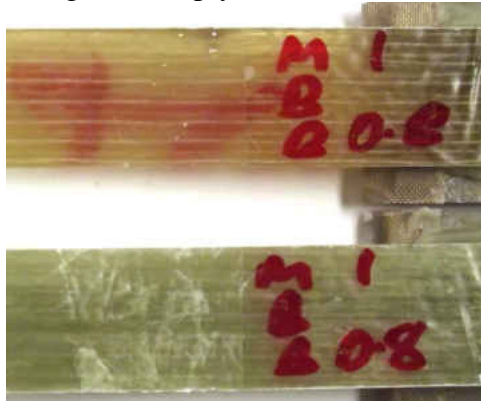
(f) Partial ply NRR4' $G_{II}/G=0.2$



(g) Partial ply MB-B $G_{II}/G=0.5$



(h) Partial ply NRR4' $G_{II}/G=0.5$



(i) 1 ply MB-B $G_{II}/G=0.8$

The fractured surfaces of all specimens repaired with NRR4' resin show marked regions of fiber bridging and shear deformation of the repair resin under mode II loads. This is reflected in the higher fracture toughness values obtained for the NRR4' repair resin. In

mode I testing the fibers in the bridging zone are mainly acted upon by tensile forces and they slow down crack growth. But in the case of high shear loads they break easily, thus letting cracks propagate fast at the bonded interface. Thus even though fiber bridging was present, propagation fracture toughness values could not be attained for mixed mode I – mode II testing.

Conclusions

For the specimen configuration and dimensions ($h \sim 9$ mm) similar to those of mode I testing specimens, NRR4 had better crack propagation fracture toughness values than MB-B and better crack initiation fracture toughness values than both MB-B and NRR6. The crack initiation fracture toughness values for NRR6 were more than those for MB-B. Crack propagation fracture toughness values for NRR6 could not be recorded. A higher resolution moving camera is required for that.

For subsequent testing, fracture toughness values of NRR4' (modified NRR4) were evaluated against those for MB-B with different specimen configuration and repair parameters. It was found that repairs carried out with NRR4' are better than those conducted with repair resin MB-B.

Furthermore, repairs done after grinding off the top ply of the parent composite part partially provide higher mixed mode I – mode II fracture toughness values as compared to those conducted after grinding off one complete top ply. Since repairs on wind turbine blades damaged while in service are carried out in the field with the blades still attached to the wind turbine main support, it is difficult to maintain a constant grinding depth. Visual signs, such as reaching the backing of a ply or encountering cross weave while grinding are recorded as markers for gaging the depth ground. Future work is proposed

that can involve finding a suitable grinding depth of the top parent ply to achieve optimum fracture toughness and some means to have the top ply ground to that depth consistently every time before repairs are carried out.

Chapter V

CONCLUSIONS

In the first part of this work, mechanical characterization was conducted to select a new repair resin for a global wind turbine blade manufacturing company. It was found that NRR4, the vinyl ester resin with a higher amount of styrene, performed better than the polyester and other vinyl ester options that were selected as new repair resin candidates. A typical vinyl ester molecule consists of a main epoxy chain with unsaturated carbon – carbon double bond groups connected to its two ends with the help of ester groups. Just as in the case of unsaturated polyesters, these carbon – carbon double bonds are potential sites for crosslinking. Initiators like methyl ethyl ketone peroxide (MEKP) provide free radicals during cross linking that react at the double bond site (Figure 5.1) to form a new

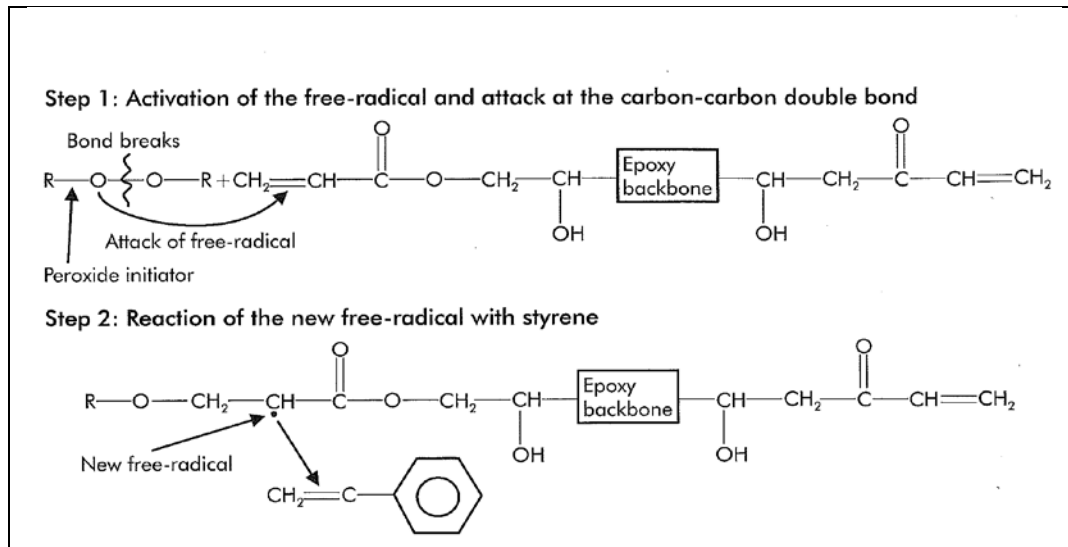
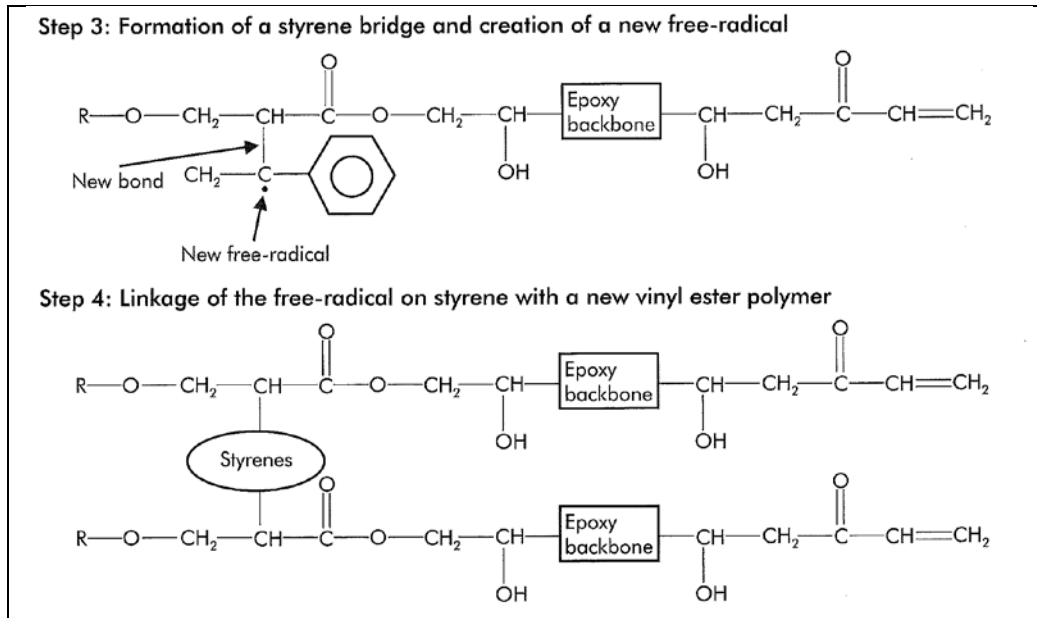


Figure 5.1. Crosslinking in vinyl ester resins [84]

Figure 5.1 cont.



free radical at that site. These free radicals further react with styrene molecules that are dispersed in the vinyl ester resin as shown in Step 3 in Figure 5.1. Depending on the relative concentration of styrene molecules in the resin, short or long chains consisting of styrene molecules are formed before they attach themselves to another vinyl ester molecule. The carbon – carbon double bond groups that have not yet reacted may join to other similar unsaturated parts of vinyl ester molecules through similar styrene bridges thus resulting in a large cross – linked system. The extent of cross linking depends upon the temperature at which the resin is cured. Usually, at room temperature after initial crosslinking, mobility of the polymer chains gets limited and the rate of crosslinking reduces. Some unsaturated (carbon – carbon double bond) groups that do not react at all are still left in the system. Post curing is carried out to fully cure the resin. The composite is generally post cured at a temperature that is higher than the glass transition temperature of the resin. As the polymer chains become more mobile, the rate of crosslinking

increases and this results in reduction in sites of unsaturation. This in turn increases the glass transition temperature of the resin and eventually the resin gets fully cured at a point when the glass transition temperature equals the post curing temperature. If the resin is heated further there is a degradation in the mechanical strength of the composite. When cured at room temperature, NRR4 was determined to have a degree of cure of 54.4% through differential scanning calorimetry. To ensure that there was no degradation in the mechanical properties of the repair resin, NRR4 was post cured at a temperature that was below its glass transition temperature and thus it was not still fully cured after post curing.

When an initiated repair resin similar to NRR4 containing styrene is applied to a pre – cured polymer surface, there is diffusion of styrene as well as resin into the cured polymer [75]. The amount of the diffusion depends on factors such as time of exposure, temperature, molecular weight, concentration, etc. Based on the difference in molecular weights, the coefficient of diffusion of styrene is about an order higher than that of the resin [75]. Though the exact amount of styrene in the repair resin NRR4 is not known due to proprietary reasons, it is known that the amount of styrene in NRR4 is greater than that in the other repair resin candidates. It may be safely assumed that since the diffusion of styrene into the parent plates is proportional to its content in the different resins, it diffuses more in the case of NRR4. The newly diffused styrene molecules have a tendency to form links with the unreacted double bonds in the parent plates and also with those in the repair resin thus creating a crosslink structure across the repair interface. More quantity of absorbed styrene molecules reflects a more complex crosslink structure. This leads to higher fracture toughness values as were recorded in the case of NRR4.

The fracture toughness testing of repairs conducted on surfaces with varying top ply grinding depths revealed some interesting results. It was found that the repairs acted better when conducted on a surface that consisted of a mixture of pre-cured resin and exposed fibers than when carried out on a surface with only pre-cured resin. Pronounced fiber bridging was observed in the former case as the exposed fibers got bonded to the repair resin and this resulted in the higher fracture toughness values observed. These exposed fibers that bonded to the repair resin also hindered crack propagation. When the repair surface consisted mainly of pre-cured resin, the repair resin bonded with it only and no or very little fibers were present at the bond-line. This resulted in almost no fiber bridging and the fracture toughness values thus obtained were lower. This phenomenon was observed in Mode I crack propagation fracture toughness testing and then again in Mixed Mode I – Mode II crack initiation fracture toughness tests.

The commonly used method of conducting repairs on engineering composites (low modulus composites) involves grinding out the region with the damaged portion and then completely removing the top-most ply below the damaged portion through grinding. The repairs are then carried out on this surface. From the results of the varying grinding depth study it seems that in order to improve repair fracture toughness, it might be helpful not to grind the repair surface layer off completely. The repairs conducted this way showed an improvement in fracture toughness values when tested under Mode I and Mixed Mode I – Mode II loading. Fatigue characterization of such repairs would provide a further insight into their performance. It can further be investigated whether the depth to which the repair surface ply is ground down has any effect on the strength of repairs.

Reinforcement manufacturers coat the fibers with polymeric materials called sizings. These coatings have multiple purposes such as protecting the fibers from mechanical damage and environmental degradation, providing desirable fabric qualities and improving bond strength between matrix and reinforcement. The sizings used for fiberglass generally consist of polymeric molecules with a silicon group (glass friendly) at one end and an organic group compatible with the resin at the other. This arrangement helps in strengthening the bonds between the polymer matrix and fiberglass and in turn improving the overall strength and stiffness of the composite. When the composite surface top ply is partially ground down for repairs, the sizing may be partially or completely removed from the surface of the exposed fibers. When repairs are conducted over this surface the interfacial strength between these exposed fibers and the repair resin is less as compared to that between fibers and matrix in the parent plate. Due to reduction in the interfacial strength, the fibers peel off easily from the matrix rather than breaking. This results in an increase in fiber bridging during crack propagation and thus greater fracture toughness values are obtained. Feih *et al* [85] established that the fracture toughness of the composite improves substantially when the fiber reinforced composite is made with fibers with the sizing removed. Though there is an improvement in the fracture toughness values due to removal of sizing, this makes the fibers more susceptible to mechanical damage and environmental and chemical attacks. The strength and stiffness of the composite are also compromised. A deeper study of this phenomenon can involve determination of the extent of sizing removal due to grinding and the resulting decrease in the bond strength between the fibers and the matrix and the effect on fracture

toughness, stiffness and strength of repairs. The amount of degradation of fiber properties can also be evaluated.

The studies proposed above would be conducive to the overall betterment of the repair process carried out by companies that manufacture parts with fiberglass composites.

REFERENCES

- [1] J. Cinquin, Composites in Aerospace. Engineering Techniques, 2002:AM5645.
- [2] J. Moutier, M. Fois, C. Picard, Characterization of carbon/epoxy materials for structural repair of carbon/BMI structures, Composites Part B: Engineering, Volume 40, Issue 1, January 2009, Pages 1-6, ISSN 1359-8368.
- [3] D. Tzetzis, P.J. Hogg, Experimental and finite element analysis on the performance of vacuum-assisted resin infused single scarf repairs, Materials & Design, Volume 29, Issue 2, 2008, Pages 436-449, ISSN 0261-3069.
- [4] Hexcel Composites, Composite Repair. Publication No. UTC 102, April 1999
- [5] J. Wang, Z. Zhou, R. Vodicka, W.K. Chiu, Selection of patch and adhesive materials for helicopter battle damage repair applications, Composite Structures, Volume 91, Issue 3, December 2009, Pages 278-285, ISSN 0263-8223.
- [6] Det Norske Veritas and Risø National Laboratory, Guidelines for Design of Wind Turbines, 2nd Edition, Copenhagen: Det Norske Veritas/Risø, 2002.
- [7] International Electrotechnical Commission, IEC 61400-1, Wind Turbines – Part 1, Design Requirements, Edition 3 (2005).
- [8] International Electrotechnical Commission, IEC 61400-23, Technical Specification, Wind Turbine Generator Systems – Part: 23, Full-Scale Structural Testing of Rotor Blades (2001).
- [9] Det Norske Veritas, Offshore Standard DNV-OS-J101 Design of Offshore Wind Turbine Structures, Det Norske Veritas, Høvik, Norway (2004).

- [10] Det Norske Veritas, Offshore Standard DNV-OS-J102 Design and Manufacture of Wind Turbine Blades, Offshore and Onshore Wind Turbines, Det Norske Veritas, Høvik, Norway (2006).
- [11] Germanische Lloyd, Guideline for the Certification of Wind Turbines, Germanische Lloyd, Hamburg, Germany (2003 with Supplement 2004).
- [12] Germanische Lloyd, Guideline for the Certification of Offshore Wind Turbines, Germanische Lloyd, Hamburg, Germany (2005).
- [13] J.W. Holmes, B.F. Sørensen, P. Brondsted. Reliability of wind turbine blades: An overview of materials testing. Wind Power Shanghai 2007, proceedings
- [14] T. K. O'Brien, W. M. Johnston , G. J. Toland. Mode II interlaminar fracture toughness and fatigue characterization of a graphite epoxy composite material. NASA/TM-2010-216838, 2010.
- [15] ASTM Standard D3479/D3479M, 2012, "Standard Test Method for Tension-Tension fatigue of Polymer Matrix Composite Materials" ASTM International, West Conshohocken, PA, 2012, DOI: 10.1520/D3479_D3479M-12, www.astm.org.
- [16] ASTM Standard D6115-97(2011), 2011, "Standard Test Method for Mode I Fatigue Delamination Growth Onset of Unidirectional Fiber-Reinforced Polymer Matrix Composites" ASTM International, West Conshohocken, PA, 2011, DOI: 10.1520/D6115-97R11, www.astm.org.
- [17] V. V. Bolotin. Mechanics of delaminations in laminate composite structures. Mechanics of Composite Materials 2001; 37(5/6): 367–380.
- [18] ASTM Standard D5528 – 01(2007) e3, “Standard Test Method for Mode I Interlaminar Fracture Toughness of Unidirectional Fiber-Reinforced Polymer Matrix

Composites”, ASTM International, West Conshohocken, PA, 2007, DOI: 10.1520/D5528-01R07E03, (www.astm.org).

[19] Anon. Protocol for interlaminar testing of composites. Delft, The Netherlands: European Structural Integrity Society, 1993.

[20] Anon. Testing methods for interlaminar fracture toughness of carbon fiber reinforced plastics (JIS K 7086-1993). Tokyo, Japan: Japanese Industrial Standards Group, 1993.

[21] ISO 15024, Fiber-reinforced Plastic Composites – Determination of Mode I Interlaminar Fracture Toughness, G_{Ic} , for Unidirectionally Reinforced Materials (2001).

[22] A. Refahi Oskouei, A. Zucchelli, M. Ahmadi, G. Minak. An integrated approach based on acoustic emission and mechanical information to evaluate the delamination fracture toughness at mode I in composite laminate. *Mater Des* 2011;32:1444–55.

[23] F. Perrin, M.N Bureau, J. Denault, J.I. Dickson, Mode I interlaminar crack propagation in continuous glass fiber/polypropylene composites: temperature and molding condition dependence, *Composites Science and Technology*, Volume 63, Issue 5, April 2003, Pages 597-607, ISSN 0266-3538.

[24] D. Tzetzis, P.J. Hogg, Bondline toughening of vacuum infused composite repairs, *Composites Part A: Applied Science and Manufacturing*, Volume 37, Issue 9, September 2006, Pages 1239-1251, ISSN 1359-835X.

[25] M.G Bader, I Hamerton, J.N Hay, M Kemp, S Winchester, Double cantilever beam testing of repaired carbon fibre composites, *Composites Part A: Applied Science and Manufacturing*, Volume 31, Issue 6, June 2000, Pages 603-608, ISSN 1359-835X.

[26] J.H. Chen, E. Schulz, J. Bohse, G. Hinrichsen, Effect of fibre content on the interlaminar fracture toughness of unidirectional glass-fibre/polyamide composite,

Composites Part A: Applied Science and Manufacturing, Volume 30, Issue 6, June 1999, Pages 747-755, ISSN 1359-835X.

[27] A.A. Baker, Repair of cracked or defective metallic aircraft components with advanced fibre composites—an overview of Australian work, Composite Structures, Volume 2, Issue 2, 1984, Pages 153-181, ISSN 0263-8223.

[28] Turaga V.R.S. Umamaheswar, Ripudaman Singh, Modelling of a patch repair to a thin cracked sheet, Engineering Fracture Mechanics, Volume 62, Issues 2–3, January–February 1999, Pages 267-289, ISSN 0013-7944.

[29] D. O. Hammond, J. B. Cochran, Composite Material Repairs to Metallic Airframe Components, USAF Structural Integrity program Conference, September 1993, Page(s) 32, ADA272876, MMCIA/F012315-31.

[30] C.-L. Ong, S.B. Shen, The reinforcing effect of composite patch repairs on metallic aircraft structures, International Journal of Adhesion and Adhesives, Volume 12, Issue 1, January 1992, Pages 19-26, ISSN 0143-7496.

[31] R. Jones, R. Bartholomeusz, R. Kaye, J. Roberts, Bonded-composite repair of representative multi-site damage in a full-scale fatigue-test article, Theoretical and Applied Fracture Mechanics, Volume 21, Issue 1, August 1994, Pages 41-49, ISSN 0167-8442.

[32] A.A. Baker, Fibre composite repair of cracked metallic aircraft components — practical and basic aspects, Composites, Volume 18, Issue 4, September 1987, Pages 293-308, ISSN 0010-4361.

- [33] Yail J. Kim, Kent A. Harries, Fatigue behavior of damaged steel beams repaired with CFRP strips, *Engineering Structures*, Volume 33, Issue 5, May 2011, Pages 1491-1502, ISSN 0141-0296.
- [34] Michael L. Overd, Carbon composite repairs of helicopter metallic primary structures, *Composite Structures*, Volume 25, Issues 1–4, 1993, Pages 557-565, ISSN 0263-8223.
- [35] A.A. Baker, R.J. Callinan, M.J. Davis, R. Jones, J.G. Williams, Repair of mirage III aircraft using the BFRP crack-patching technique, *Theoretical and Applied Fracture Mechanics*, Volume 2, Issue 1, October 1984, Pages 1-15, ISSN 0167-8442.
- [36] T. J. Reinhart, Bonded composite doublers used in the repair of cracked metallic structure: Proc. Conf. Advanced Composites Technologies, Dearborn, MI, USA 8–11 Nov. 1993, pp. 533–541, *International Journal of Fatigue*, Volume 16, Issue 8, 1994, Page 593, ISSN 0142-1123.
- [37] C.L. Ong, S.B. Shen, Repair of F-104 aircraft nosedome by composite patching, *Theoretical and Applied Fracture Mechanics*, Volume 15, Issue 1, May 1991, Pages 75-83, ISSN 0167-8442.
- [38] Hossein Hosseini-Toudeshky, Mir Ali Ghaffari, Bijan Mohammadi, Finite element fatigue propagation of induced cracks by stiffeners in repaired panels with composite patches, *Composite Structures*, Volume 94, Issue 5, April 2012, Pages 1771-1780, ISSN 0263-8223.
- [39] Dae-Cheol Seo, Jung-Ju Lee, Fatigue crack growth behavior of cracked aluminum plate repaired with composite patch, *Composite Structures*, Volume 57, Issues 1–4, July 2002, Pages 323-330, ISSN 0263-8223.

- [40] V. Sabelkin, S. Mall, J.B. Avram, Fatigue crack growth analysis of stiffened cracked panel repaired with bonded composite patch, *Engineering Fracture Mechanics*, Volume 73, Issue 11, July 2006, Pages 1553-1567, ISSN 0013-7944.
- [41] Hongbo Liu, Riadh Al-Mahaidi, Xiao-Ling Zhao, Experimental study of fatigue crack growth behaviour in adhesively reinforced steel structures, *Composite Structures*, Volume 90, Issue 1, September 2009, Pages 12-20, ISSN 0263-8223.
- [42] R. Jones, K. Krishnapillai, S. Pitt, Crack patching: Predicting fatigue crack growth, *Theoretical and Applied Fracture Mechanics*, Volume 45, Issue 2, April 2006, Pages 79-91, ISSN 0167-8442.
- [43] Nicholas G. Tsouvalis, Lazarus S. Mirisiotis, Dimitris N. Dimou, Experimental and numerical study of the fatigue behaviour of composite patch reinforced cracked steel plates, *International Journal of Fatigue*, Volume 31, Issue 10, October 2009, Pages 1613-1627, ISSN 0142-1123.
- [44] Q.Y. Wang, R.M. Pidaparti, Static characteristics and fatigue behavior of composite-repaired aluminum plates, *Composite Structures*, Volume 56, Issue 2, May 2002, Pages 151-155, ISSN 0263-8223.
- [45] Yi-Ming Jen, Fatigue life evaluation of adhesively bonded scarf joints, *International Journal of Fatigue*, Volume 36, Issue 1, March 2012, Pages 30-39, ISSN 0142-1123.
- [46] A. Bernasconi, A. Jamil, F. Moroni, A. Pironi, A study on fatigue crack propagation in thick composite adhesively bonded joints, *International Journal of Fatigue*, Volume 50, May 2013, Pages 18-25, ISSN 0142-1123.

- [47] H.S. da Costa Mattos, A.H. Monteiro, R. Palazzetti, Failure analysis of adhesively bonded joints in composite materials, *Materials & Design*, Volume 33, January 2012, Pages 242-247, ISSN 0261-3069.
- [48] M.V. Fernández, M.F.S.F. de Moura, L.F.M. da Silva, A.T. Marques, Composite bonded joints under mode I fatigue loading, *International Journal of Adhesion and Adhesives*, Volume 31, Issue 5, July 2011, Pages 280-285, ISSN 0143-7496.
- [49] Maria V. Fernández, Marcelo F.S.F. de Moura, Lucas F.M. da Silva, António T. Marques, Characterization of composite bonded joints under pure mode II fatigue loading, *Composite Structures*, Volume 95, January 2013, Pages 222-226, ISSN 0263-8223.
- [50] M.V. Fernández, M.F.S.F. de Moura, L.F.M. da Silva, A.T. Marques, Mixed-mode I + II fatigue/fracture characterization of composite bonded joints using the Single-Leg Bending test, *Composites Part A: Applied Science and Manufacturing*, Volume 44, January 2013, Pages 63-69, ISSN 1359-835X.
- [51] Andrew Makeev, Interlaminar shear fatigue behavior of glass/epoxy and carbon/epoxy composites, *Composites Science and Technology*, Volume 80, 17 May 2013, Pages 93-100, ISSN 0266-3538.
- [52] S. Stelzer, A.J. Brunner, A. Argüelles, N. Murphy, G. Pinter, Mode I delamination fatigue crack growth in unidirectional fiber reinforced composites: Development of a standardized test procedure, *Composites Science and Technology*, Volume 72, Issue 10, 8 June 2012, Pages 1102-1107, ISSN 0266-3538.

- [53] M. Abo-Elkhier, A.A. Hamada, A. Bahei El-Deen, Prediction of fatigue life of glass fiber reinforced polyester composites using modal testing, *International Journal of Fatigue*, Available online 22 October 2012, ISSN 0142-1123.
- [54] N.K. Kar, Y. Hu, E. Barjasteh, S.R. Nutt, Tension–tension fatigue of hybrid composite rods, *Composites Part B: Engineering*, Volume 43, Issue 5, July 2012, Pages 2115-2124, ISSN 1359-8368.
- [55] Mehmet Emin Deniz, Mustafa Ozen, Okan Ozdemir, Ramazan Karakuzu, Bulent Murat Icten, Environmental effect on fatigue life of glass–epoxy composite pipes subjected to impact loading, *Composites Part B: Engineering*, Volume 44, Issue 1, January 2013, Pages 304-312, ISSN 1359-8368.
- [56] Kahirdeh, A., Naderi, M., & Khonsari, M. (2012). On the role of cooling on fatigue failure of a woven glass/epoxy laminate. *Journal of Composite Materials*, doi:10.1177/0021998312451608
- [57] Huh Y. H., Lee J. H., Kim D. J., Lee Y. S., Effect of stress ratio on fatigue life of GFRP composites for WT blade, *Journal of Mechanical Science and Technology*, April 2012, doi:10.1007/s12206-012-0526-0
- [58] Christoph W. Kensche, Fatigue of composites for wind turbines, *International Journal of Fatigue*, Volume 28, Issue 10, October 2006, Pages 1363-1374, ISSN 0142-1123.
- [59] V. Dattoma, S. Giancane, Evaluation of energy of fatigue damage into GFRC through digital image correlation and thermography, *Composites Part B: Engineering*, Volume 47, April 2013, Pages 283-289, ISSN 1359-8368.

- [60] M.A. Caminero, S. Pavlopoulou, M. Lopez-Pedrosa, B.G. Nicolaisson, C. Pinna, C. Soutis, Analysis of adhesively bonded repairs in composites: Damage detection and prognosis, *Composite Structures*, Volume 95, January 2013, Pages 500-517, ISSN 0263-8223.
- [61] ASTM D 6671 – 06, “Standard Test Method for Mixed Mode I – Mode II Interlaminar Fracture Toughness of Unidirectional Fiber Reinforced Polymer Matrix Composites”, ASTM International, West Conshohocken, PA, 2006, DOI: 10.1520/D6671M-06, www.astm.org.
- [62] S. Singh, I.K. Partridge, Mixed-mode fracture in an interleaved carbon-fibre/epoxy composite, *Composites Science and Technology*, Volume 55, Issue 4, 1995, Pages 319-327, ISSN 0266-3538.
- [63] P. Naghipour, J. Schneider, M. Bartsch, J. Hausmann, H. Voggenreiter, Fracture simulation of CFRP laminates in mixed mode bending, *Engineering Fracture Mechanics*, Volume 76, Issue 18, December 2009, Pages 2821-2833, ISSN 0013-7944.
- [64] Feret, Victor, Hossein Ghiasi, and Pascal Hubert. "Effect of Fibre Volume Fraction on Mixed-Mode Fracture of a Fabric Carbon/Epoxy Composite." *Applied Composite Materials* (2012): 1-15.
- [65] X. Fan, Q. Sun, Study on Mixed-mode Interlaminar Fracture of Laminated Composites, *Applied Mechanics and Materials Vols. 110-116* (2012) pp 1345-1352, doi:10.4028/www.scientific.net/AMM.110-116.1345
- [66] M.L. Benzeggagh, M. Kenane, Measurement of mixed-mode delamination fracture toughness of unidirectional glass/epoxy composites with mixed-mode bending apparatus,

Composites Science and Technology, Volume 56, Issue 4, 1996, Pages 439-449, ISSN 0266-3538.

[67] F. Ducept, P. Davies, D. Gamby, An experimental study to validate tests used to determine mixed mode failure criteria of glass/epoxy composites, *Composites Part A: Applied Science and Manufacturing*, Volume 28, Issue 8, 1 June 1997, Pages 719-729, ISSN 1359-835X.

[68] F. Ducept, D. Gamby, P. Davies, A mixed-mode failure criterion derived from tests on symmetric and asymmetric specimens, *Composites Science and Technology*, Volume 59, Issue 4, March 1999, Pages 609-619, ISSN 0266-3538

[69] F. Ducept, P. Davies, D. Gamby, Mixed mode failure criteria for a glass/epoxy composite and an adhesively bonded composite/composite joint, *International Journal of Adhesion and Adhesives*, Volume 20, Issue 3, 2000, Pages 233-244, ISSN 0143-7496.

[70] F. Dharmawan, G. Simpson, I. Herszberg, S. John, Mixed mode fracture toughness of GFRP composites, *Composite Structures*, Volume 75, Issues 1–4, September 2006, Pages 328-338, ISSN 0263-8223.

[71] Rosa M. Marat-Mendes, Manuel M. Freitas, Failure criteria for mixed mode delamination in glass fibre epoxy composites, *Composite Structures*, Volume 92, Issue 9, August 2010, Pages 2292-2298, ISSN 0263-8223.

[72] S. P. Blake, K. A. Berube, R. A. Lopez-Anido, (2012). Interlaminar fracture toughness of woven E-glass fabric composites. *Journal of Composite Materials*, 46(13), 1583-1592.

[73] Rosa Marat-Mendes, M. de Freitas, Characterisation of the edge crack torsion (ECT) test for the measurement of the mode III interlaminar fracture toughness, *Engineering*

Fracture Mechanics, Volume 76, Issue 18, December 2009, Pages 2799-2809, ISSN 0013-7944.

[74] J. R. Reeder. 3D mixed mode delamination fracture criteria – an experimentalist's perspective. In: Proceedings of American Society for Composites, 21st annual technical conference, Dearborn, MI, United States, 17–20 September; 2006.

[75] J. Ben Abdelouahab, J. M. Vergnaud, Diffusion of styrene and polyester in thermosets and application in repairing broken thermoset pieces, Polymer Testing, Volume 22, Issue 2, April 2003, Pages 203-208, ISSN 0142-9418.

[76] M. R. Moghbeli, F. Bakhshandeh, M. Ahmadi, Poly(n-butyl acrylate)/poly(vinyl acetate-co-methyl methacrylate) structural rubber latex particles as impact modifier for unsaturated polyester resin: Preparation and characterization, Iranian Polymer Journal (English Edition), Volume 20, Issue 7, 2011, Pages 607-617.

[77] V. Mollón, J. Bonhomme, J. Viña, A. Argüelles, Theoretical and experimental analysis of carbon epoxy asymmetric dcB specimens to characterize mixed mode fracture toughness, Polymer Testing, Volume 29, Issue 6, September 2010, Pages 766-770, ISSN 0142-9418.

[78] A. SILVA, M. J. MOREIRA DE FREITAS, Mixed-mode delamination growth of laminar composites by using three-dimensional finite element modeling. Fatigue & Fracture of Engineering Materials & Structures, Volume 26, 2003, Pages 543–549.

[79] A. B. Pereira, A. B. de Moraes, Mixed mode I+II interlaminar fracture of carbon/epoxy laminates, Composites Part A: Applied Science and Manufacturing, Volume 39, Issue 2, February 2008, Pages 322-333, ISSN 1359-835X.

- [80] J.W. Hutchinson, Z. Suo, Mixed Mode Cracking in Layered Materials, In: John W. Hutchinson and Theodore Y. Wu, Editor(s), Advances in Applied Mechanics, Elsevier, 1991, Volume 29, Pages 63-191, ISSN 0065-2156.
- [81] H. Elbishari, N. Silikas, J. Satterthwaite, Filler size of resin-composites, percentage of voids and fracture toughness: Is there a correlation? Dental Materials Journal, 2012, Volume 31, Issue 4, Pages 523-527.
- [82] M. A. El-Hadek, H. V. Tippur, Simulation of porosity by microballoon dispersion in epoxy and urethane: Mechanical measurements and models, Journal of Materials Science, 2002, Volume 37, Issue 8, Pages 1649-1660.
- [83] Fibre-reinforced plastics -- Determination of fatigue properties under cyclic loading conditions. BS ISO 13303:2003. ISO/TC 61/SC 13. ICS: 83.120
- [84] Strong, A. B. (2008), Fundamentals of Composites Manufacturing Materials, Methods and Applications. Dearborn: Society of Manufacturing Engineers (SME).
- [85] S. Feih, J. Wei, P. Kingshott, B.F. Sørensen, The influence of fibre sizing on the strength and fracture toughness of glass fibre composites, Composites Part A: Applied Science and Manufacturing, Volume 36, Issue 2, February 2005, Pages 245-255, ISSN 1359-835X